Pan-LUT: Efficient Pan-sharpening via Learnable Look-Up Tables

Zhongnan Cai[1*] **Yingying Wang**[1*] **Hui Zheng**[1] **Panwang Pan**[2]
ZiXu Lin[1] **Ge Meng**[1] **Chenxin Li**[3] **Chunming He**[4]
Jiaxin Xie[1] **Yunlong Lin**[1†] **Junbin Lu**[5] **Yue Huang**[1] **Xinghao Ding**[1‡]
[1]Key Laboratory of Multimedia Trusted Perception and Efficient Computing,
Ministry of Education of China, Xiamen University, Xiamen, Fujian, China
[2]ByteDance [3]The Chinese University of Hong Kong
[4]Duke University [5]University of Washington

Abstract

Recently, deep learning-based pan-sharpening algorithms have achieved notable advancements over traditional methods. However, deep learning-based methods incur substantial computational overhead during inference, especially with large images. This excessive computational demand limits the applicability of these methods in real-world scenarios, particularly in the absence of dedicated computing devices such as GPUs and TPUs. To address these challenges, we propose Pan-LUT, a novel learnable look-up table (LUT) framework for pan-sharpening that strikes a balance between performance and computational efficiency for large remote sensing images. Our method makes it possible to process 15K$\times$15K remote sensing images on a 24GB GPU. To finely control the spectral transformation, we devise the PAN-guided look-up table (PGLUT) for channel-wise spectral mapping. To effectively capture fine-grained spatial details, we introduce the spatial details look-up table (SDLUT). Furthermore, to adaptively aggregate channel information for generating high-resolution multispectral images, we design an adaptive output look-up table (AOLUT). Our model contains fewer than 700K parameters and processes a 9K$\times$9K image in under 1 ms using one RTX 2080 Ti GPU, demonstrating significantly faster performance compared to other methods. Experiments reveal that Pan-LUT efficiently processes large remote sensing images in a lightweight manner, bridging the gap to real-world applications. Furthermore, our model surpasses SOTA methods in full-resolution scenes under real-world conditions, highlighting its effectiveness and efficiency. The source code is available at `https://github.com/CZhongnan/Pan-LUT`.

1 Introduction

High-resolution multispectral (HRMS) images are widely used in applications such as military operations, environmental monitoring, and mapping. However, due to the limitations of physical sensors, these images are challenging to obtain. Pan-sharpening addresses this issue by fusing high-resolution panchromatic (PAN) images with low-resolution multispectral (LRMS) images, producing high-quality HRMS images through complementary integration [62] [68] [49]. Recently, numerous pan-sharpening methods have been proposed, which can be generally categorized into two main groups: traditional methods and deep learning-based methods. Traditional methods,

[*]Equal Contribution.
[†]Project Leader.
[‡]Corresponding author.

39th Conference on Neural Information Processing Systems (NeurIPS 2025).

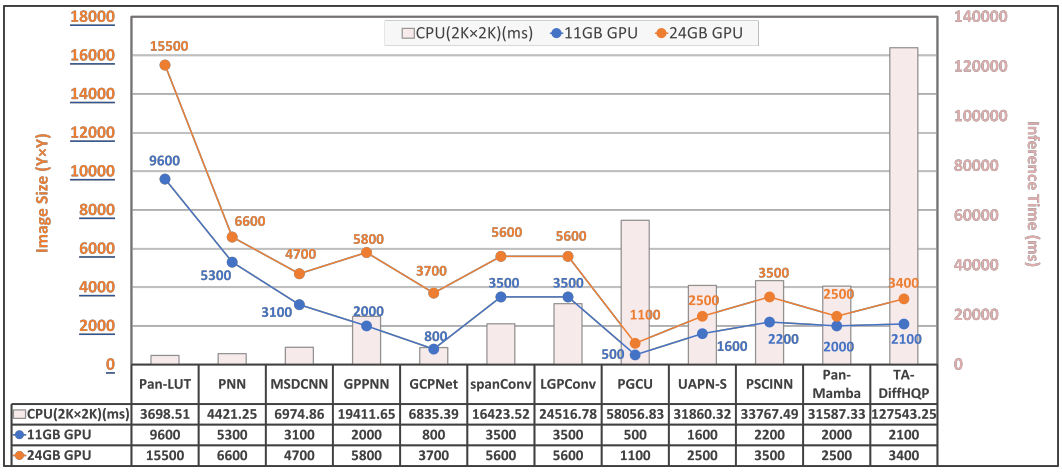

	Pan-LUT	PNN	MSDCNN	GPPNN	GCPNet	spanConv	LGPConv	PGCU	UAPN-S	PSCINN	Pan-Mamba	TA-DiffHQP
CPU(2K×2K)(ms)	3698.51	4421.25	6974.86	19411.65	6835.39	16423.52	24516.78	58056.83	31860.32	33767.49	31587.33	127543.25
11GB GPU	9600	5300	3100	2000	800	3500	3500	500	1600	2200	2000	2100
24GB GPU	15500	6600	4700	5800	3700	5600	5600	1100	2500	3500	2500	3400

Figure 1: **Comparisons of computational efficiency.** Our method can process 9K×9K and 15K×15K images on GPUs with 11GB and 24GB memory, respectively. Meanwhile, we observe that (a) DNN-based methods are highly sensitive to the image size, and (b) in the absence of a GPU, they require a considerable amount of time to process images. In the CPU inference time experiments, all methods were conducted on a workstation equipped with an Intel(R) Xeon(R) Gold 6226R CPU.

such as component substitution (CS) [4] [5] [14], multi-resolution analysis (MRA) [10] [22], and variational optimization (VO) [13] [41], often struggle to restore precise spatial or spectral details in HRMS images. In contrast, deep learning-based pan-sharpening methods have demonstrated exceptional fusion capabilities due to the powerful feature extraction ability of deep neural networks (DNNs) [28] [29] [32] [33]. Masi et al. [38] built the Pan-sharpening Neural Network (PNN) model, which first applied CNN to pan-sharpening field, achieving a significant improvement over traditional methods. Following this, researchers have explored more complicated and deeper networks to further promote the performance of pan-sharpening [16] [30] [39] [63]. However, they overlook a critical practical issue: the need for real-time processing of large remote sensing images in real-world applications. As illustrated in Figure 1, we observe two major limitations in DNN-based approaches: (1) they are highly sensitive to the size of the input images, and (2) they rely heavily on dedicated computing devices such as GPUs and TPUs. Increasing GPU memory does not significantly improve the image size these methods can handle and several of these methods demand a significant amount of time to process images in CPU-only environments. And we will demonstrate in the experiments sections that, even with GPU acceleration, most methods still fail to process large remote sensing images in real time. In practical applications, remote sensing images typically exhibit even higher resolutions, posing additional challenges to existing methods in terms of efficiency and scalability. Moreover, simply increasing network depth does not necessarily lead to better performance, as deeper models are harder to train and often suffer from overfitting due to redundant parameters.

To overcome the aforementioned challenges, we propose a novel learnable Look-Up Table (LUT) framework, called Pan-LUT, which achieves a good balance between performance and computational efficiency in pan-sharpening. Specifically, we replace complex DNN operations with learnable LUTs to enable lightweight deployment in practical applications. To finely control the spectral transformation, we devise the PAN-guided look-up table (PGLUT) for channel-wise spectral mapping. To effectively capture fine-grained spatial details, we introduce the spatial details look-up table (SDLUT). To further enable adaptive channel aggregation for high-resolution multispectral image generation, we design the adaptive output look-up table (AOLUT). The Pan-LUT consists of fewer than 700K parameters and can processes 9K×9K images in under 1 ms using a single RTX 2080 Ti GPU. Furthermore, our approach outperforms traditional methods by 7 dB, while maintaining a speed comparable to that of conventional techniques, demonstrating superior speed and efficiency compared to existing methods. Our contributions can be summarized as follows:

- We present Pan-LUT, a novel learnable LUT framework that does not incorporate any network structure. This framework is designed to achieve a strong balance between performance and computational efficiency in pan-sharpening high-resolution remote sensing

images. Our method makes it possible to process 15K×15K remote sensing images on one 24GB GPU.

- To finely control the spectral transformation, we devise the PAN-guided look-up table (PGLUT) for channel-wise spectral mapping. To effectively capture fine-grained spatial details and adaptively learn local contexts, we introduce the spatial details look-up table (SDLUT). To further enable adaptive channel aggregation for high-resolution multispectral image generation, we design the adaptive output look-up table (AOLUT).
- To the best of our knowledge, this is the first attempt to introduce LUTs for efficient pan-sharpening. Extensive experiments on different satellite datasets demonstrate the effectiveness and efficiency of Pan-LUT.

2 Related Work

2.1 Look-Up Table

Look-up Tables (LUT) are particularly useful for functions of multiple variables, as they store pre-computed outputs for all possible input combinations. For example, in a 1D LUT, a single input index is mapped to an output value, often using linear interpolation for indices that fall between pre-stored values. More complex LUTs, such as 3D LUTs, use three independent input variables, which may require advanced interpolation methods like trilinear or tetrahedral interpolation. Due to its portability, various LUT based solutions have been proposed for image enhancement [9] [26] [31] [45] [59]. For instance, Zeng et al. [59] and Wang et al. [45] propose image-adaptive 3D LUTs for efficient single-image enhancement. These approaches rely on a network weight predictor to fuse different 3D LUTs, which may pose a limitation on platforms under resource-constrained conditions. Additionally, LUT-based methods have been explored in the area of super-resolution [21] [25] [36] [34]. SRLUT [21] trains a deep super-resolution (SR) network with a restricted receptive field and then cache the output values from the learned SR network in LUTs. However, issues such as performance degradation arise when large patches are cached in LUTs, prompting the development of strategies like MuLUT [25], which introduces multiple LUT variants and a fine-tuning strategy to improve performance. To further enhance the functionality of LUTs, architectures like SPLUT [36] and RCLUT [34] have been proposed. SPLUT processes different image information separately using multiple LUTs, while RCLUT introduces a plugin module to improve LUT-based models with minimal additional computational cost.

2.2 Traditional Pan-sharpening Methods

Traditional fusion techniques encompass component substitution (CS), multi-resolution analysis (MRA), and variational optimization (VO). CS methods, such as IHS [4], Brovey [14], and PCA [5], utilize spatial details from high-resolution panchromatic (PAN) images to replace corresponding details in low-resolution multispectral (LRMS) images, which can lead to spectral distortion due to the incomplete incorporation of spectral information. MRA techniques, including DWT [22] and ATWT [10], apply multi-resolution decomposition to merge PAN and LRMS images, which enables better preservation of spectral information and reduces spectral distortion. VO methods, such as Bayesian [13] and Total Variation [41], formulate the fusion process as an optimization problem by iteratively minimizing the loss function. While VO methods show promising results, they encounter challenges in optimizing model design and loss functions. Although these approaches have yielded certain improvements, their performance remains constrained by the inadequate modeling, which restricts further advancements in pan-sharpening accuracy and quality.

2.3 Deep Learning-based Methods

Deep learning-based methods have emerged as the dominant approach for pan-sharpening in recent years [46] [17] [50]. The PNN [38] model, inspired by SRCNN [11], is the first to introduce CNNs into this domain, surpassing traditional methods. Models like PanNet [56] and MSDCNN [57] further enhance performance by leveraging residual connections and multi-scale convolutions, effectively capturing high-frequency details and supporting a wide range of remote sensing applications. Since then, more complex CNN-based architectures [6] [18] [69] have been proposed in this field to improve the mapping ability of pan-sharpening. Models like GPPNN [52], MMNet [54], and ARFNet [53],

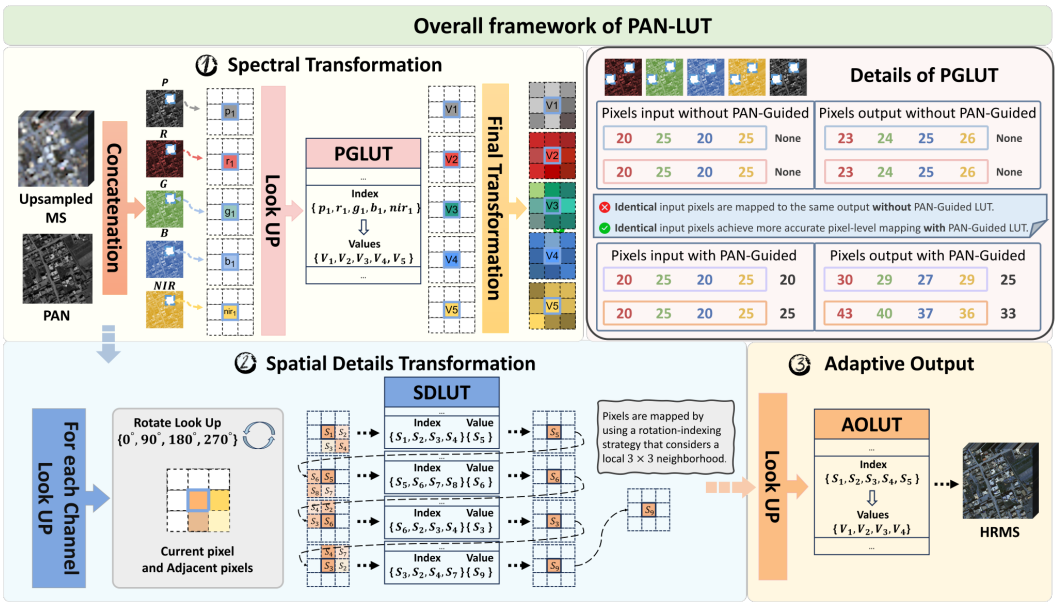

Figure 2: **The overall framework of our proposed Pan-LUT**. PGLUT is a spectral transformation LUT designed to extract spectral information, SDLUT is a spatial detail transformation LUT for capturing texture features, and AOLUT is an adaptive output LUT used to aggregate channel information.

which enhance interpretability through deep unfolding techniques and accelerate model convergence. Spatial adaptive convolution methods, such as LAGConv [20] and CANConv [12], can adaptively generate different convolution ker nel parameters based on various spatial locations, enabling them to accommodate different spatial regions. Other approaches, including SFDI [67] and MSDDN [57], utilize Fourier transforms to capture high-frequency features. Transformer-based architectures, such as INN-former [66], Panformer [64] and DRFormer [60] combine CNNs and Transformers to capture both local and global features. Instead of learning a deterministic mapping, generative models such as UCGAN [65], PanFlow [55] and PSCINN [44] generate a distribution of possible outputs for the given inputs. In addition, several studies have investigated lightweight pan-sharpening methods, including SpanConv [7] and LGPConv [61]. However, we show that current lightweight methods are only lightweight in the context of low-resolution images. Despite their promising results, these advanced methods come with high computational costs, limiting their practical applicability.

3 Method

Given the PAN image ($P \in R^{H\times W\times 1}$) and the MS image ($MS \in R^{H/r\times W/r\times C}$), pan-sharpening aims to fuse the complementary information to generate the desirable high spatial resolution MS image ($HRMS \in R^{H\times W\times C}$). Here, H and W denote the height and width of the images, r represents the spatial resolution ratio, with a value of 4, and C denotes the number of spectral bands.

3.1 Framework

The overall framework of our proposed Pan-LUT is illustrated in Figure 2, which consists of three specifically designed LUTs. (1) To finely control the spectral transformation, we devise the PAN-guided look-up table (PGLUT) for channel-wise spectral mapping, which incorporates a PAN-guided indexing strategy and a pentalinear interpolation technique. (2) To effectively capture fine-grained spatial details and adaptively learn local contexts, we introduce the spatial details look-up table (SDLUT), which incorporates a rotation-enhanced indexing strategy and a quadrilinear interpolation technique. (3) To further enable adaptive channel aggregation for high-resolution multispectral image generation, we design the adaptive output look-up table (AOLUT), which incorporates a PAN-guided indexing strategy and a pentalinear interpolation technique. Specifically, given the PAN image ($P \in \mathbb{R}^{H\times W\times 1}$) and the upsampled MS image ($MS \in \mathbb{R}^{H\times W\times C}$), they are concatenated

into $PM \in \mathbb{R}^{H\times W\times(C+1)}$ and passed through the PGLUT for channel-wise spectral mapping, producing the output $V_{pg} \in \mathbb{R}^{H\times W\times(C+1)}$. SDLUT then takes V_{pg} as input to generate local spatial details, yielding $V_{sd} \in \mathbb{R}^{H\times W\times(C+1)}$. Finally, AOLUT takes V_{sd} as input to generate the final $HRMS \in R^{H\times W\times C}$ result:

$$V_{pg} = PGLUT(PM), V_{sd} = SDLUT(V_{pg}), HRMS = AOLUT(V_{sd}). \tag{1}$$

3.2 Spectral Transformation

To preserve the rich spectral information of the MS image, we propose the PAN-guided look-up table (PGLUT), which leverages the PAN image as guidance to finely control the spectral transformation. Specifically, PGLUT is represented as a 5-dimensional matrix containing N^5 elements, where N denotes the number of bins per dimension. Each element corresponds to a sampling point, defining a set of indexed input pixels $\{I_{(i,j,k,m,n)}\}_{i,j,k,m,n=0,\dots,N-1}$ and their corresponding output pixels $\{O_{(i,j,k,m,n)}\}_{i,j,k,m,n=0,\dots,N-1}$. Here, $I \in \{pa, r, g, b, nir\}$ represents the pixel values from the PAN and MS images, while $O \in \{R, G, B, NIR\}$ denotes the corresponding cached output pixels. Since the LUT elements are discretely distributed in space, the output value cannot be directly retrieved from the LUT. For an input value $\{pa^I_{(w,h)}, r^I_{(w,h)}, g^I_{(w,h)}, b^I_{(w,h)}, nir^I_{(w,h)}\}$, where (w, h) denotes the spatial position of a pixel in the image.

PAN-guided indexing strategy. As illustrated in Figure 2, we introduce an indexing strategy for precise spectral transformation, referred to as the PAN-guided indexing strategy. In a MS image, pixels from different spatial locations may have identical values (e.g., $r_i = r_j, g_i = g_j, b_i = b_j, nir_i = nir_j$, where $i \neq j$). The LUT maps these identical inputs to the same output. The PAN-guided indexing strategy provides a more flexible indexing mechanism for the LUT. Specifically, it additionally considers the pixels at corresponding spatial positions in the PAN image (e.g., $r_i = r_j, g_i = g_j, b_i = b_j, nir_i = nir_j, pa_i \neq pa_j$, where $i \neq j$), thereby achieving finer-grained mapping. Specifically, PGLUT first performs a lookup operation to locate the corresponding input pixel in the LUT:

$$\begin{aligned} x = \frac{pa^I_{(w,h)}}{V_{max}} \cdot N, y = \frac{r^I_{(w,h)}}{V_{max}} \cdot N, z = \frac{g^I_{(w,h)}}{V_{max}} \cdot N, \\ s = \frac{b^I_{(w,h)}}{V_{max}} \cdot N, e = \frac{nir^I_{(w,h)}}{V_{max}} \cdot N, \end{aligned} \tag{2}$$

where V_{max} denotes the maximum value (e.g., 255, 1023 or 2047). The coordinates of the sampling points, $L = \{(i + c, j + c, k + c, m + c, n + c)\}$, with $c \in \{0, 1\}$, can be derived as follows:

$$i = \lfloor x \rfloor, j = \lfloor y \rfloor, k = \lfloor z \rfloor, m = \lfloor s \rfloor, n = \lfloor e \rfloor, \tag{3}$$

where $\lfloor \cdot \rfloor$ denotes the floor function. $\{\mathbf{d}_l\}_{l=x,y,z,s,e}$ represents the offset of the input index (x, y, z, s, e) relative to the defined sampling point (i, j, k, m, n), e.g., $\mathbf{d}_x = x - i$.

Pentalinear Interpolation. After locating 32 adjacent points, an appropriate interpolation technique is applied to these sampled values to generate the output:

$$O_{(x,y,z,s,e)} = PInterpolation(LUT[L], \{\mathbf{d}_l\}), \tag{4}$$

where $PInterpolation(\cdot)$ denotes the pentalinear interpolation. More details about PGLUT and the pentalinear interpolation can be found in Section A.2.

3.3 Spatial Details Transformation

PGLUT is essentially a channel-wise 5D LUT that operates globally, which limits its ability to capture local spatial information. To effectively capture fine-grained spatial details and adaptively learn local contexts, we propose the Spatial Details Lookup Table (SDLUT).

Rotation-indexing strategy. As illustrated in Figure 2, given a pixel $p_{(w,h)}$, SDLUT processes this pixel along with its neighboring pixels as input. During the training phase, we employ a Rotation-indexing strategy to further expand the receptive field, which can be formulated as:

$$\begin{aligned} p^1_{(w,h)} &= f_{SDLUT}(p_{(w,h)}, p_{(w+1,h)}, p_{(w,h+1)}, p_{(w+1,h+1)}), \\ p^2_{(w,h)} &= f_{SDLUT}(p^1_{(w,h)}, p^1_{(w+1,h)}, p^1_{(w+1,h-1)}, p^1_{(w,h-1)}), \\ p^3_{(w,h)} &= f_{SDLUT}(p^2_{(w,h)}, p^2_{(w+1,h)}, p^2_{(w,h+1)}, p^2_{(w+1,h+1)}), \\ V_{(w,h)} &= f_{SDLUT}(p^3_{(w,h)}, p^3_{(w+1,h)}, p^3_{(w,h+1)}, p^3_{(w+1,h+1)}), \end{aligned} \tag{5}$$

Table 1: Quantitative comparison across three satellite datasets. The best outcomes are highlighted in red. ↑ indicates better performance with increasing values, while ↓ signifies improved performance with decreasing values.

Method	WorldView-II				GaoFen2				Worldview-III				Param(M)	Inference (ms)	
	PSNR↑	SSIM↑	SAM↓	ERGAS↓	PSNR↑	SSIM↑	SAM↓	ERGAS↓	PSNR↑	SSIM↑	SAM↓	ERGAS↓		$2K \times 2K$	$4K \times 4K$
Brovey [14]	35.8646	0.9216	0.0403	1.8238	37.7974	0.9026	0.0218	1.3720	22.5060	0.5466	0.1159	8.2331	-	0.28	0.33
IHS [4]	35.2962	0.9027	0.0461	2.0278	38.1754	0.9100	0.0243	1.5336	22.5579	0.5354	0.1266	8.3616	-	0.23	0.26
SFIM [35]	34.1297	0.8975	0.0439	2.3449	36.9060	0.8882	0.0318	1.7398	21.8212	0.5457	0.1208	8.9730	-	0.32	0.47
GS [24]	35.6376	0.9176	0.0423	1.8774	37.2260	0.9034	0.0309	1.6736	22.5608	0.5470	0.1217	8.2433	-	0.75	0.87
PNN [38]	40.7550	0.9624	0.0259	1.0646	43.1208	0.9704	0.0172	0.8528	29.9418	0.9121	0.0824	3.3206	0.0689	12.81	54.59
PanNet [56]	40.8176	0.9626	0.0257	1.0557	43.0659	0.9685	0.0178	0.8577	29.6840	0.9072	0.0851	3.4263	0.0688	29.52	OOM
MSDCNN [57]	41.3355	0.9664	0.0242	0.9940	45.6847	0.9827	0.0135	0.6389	30.3038	0.9184	0.0782	3.1884	0.2390	49.82	OOM
Pan-GAN [37]	39.1025	0.9562	0.0303	1.2954	41.4468	0.9661	0.0205	1.0593	28.4959	0.8897	0.0998	3.9067	0.0915	40.83	OOM
GPPNN [52]	41.1622	0.9684	0.0244	1.0315	44.2145	0.9815	0.0137	0.7361	30.1785	0.9175	0.0776	3.2593	0.1198	43.60	OOM
SFDI [67]	41.7244	0.9725	0.0220	0.9506	47.4712	0.9901	0.0102	0.5462	30.5971	0.9236	0.0741	3.0798	0.0871	65.37	OOM
UCGAN [65]	40.0545	0.9553	0.0275	1.1734	42.3634	0.9557	0.0194	0.9480	28.6705	0.8851	0.0990	3.8696	0.2109	52.06	OOM
PanFlow [55]	41.8584	0.9712	0.0224	0.9335	47.2533	0.9884	0.0103	0.5512	30.4873	0.9221	0.0751	3.1142	0.0873	54.19	OOM
PSCINN [44]	41.8520	0.9703	0.0223	0.9407	47.1100	0.9878	0.0107	0.5612	30.5599	0.9230	0.0748	3.1033	3.3209	60.74	OOM
Pan-Mamba [15]	42.2354	0.9729	0.0212	0.8975	47.6453	0.9894	0.0103	0.5286	31.1551	0.9299	0.0702	2.8942	0.1827	87.74	OOM
TA-DiffHQP [47]	42.1255	0.9752	0.0211	0.9023	47.7716	0.9900	0.0101	0.5378	31.3369	0.9302	0.0737	2.6369	2.6000	998.58	OOM
Pan-LUT (**Ours**)	40.8555	0.9633	0.0254	1.0339	43.7466	0.9726	0.0169	0.8027	29.7376	0.9106	0.0815	3.3934	0.6626	**0.38**	**0.54**

where $f_{SDLUT}(\cdot)$ denotes the lookup and interpolation process in the LUT retrieval. More details about SDLUT and the quadrilinear interpolation can be found in Section A.3.

3.4 Adaptive Output

For the feature channel pixels from the SDLUT $(V^1_{(w,h)}, V^2_{(w,h)}, V^3_{(w,h)}, V^4_{(w,h)}, V^5_{(w,h)})$, AOLUT adaptively aggregates channel information to generate high-resolution multispectral channel pixels $\{R^O_{(w,h)}, G^O_{(w,h)}, B^O_{(w,h)}, NIR^O_{(w,h)}\}$. Pixel-level Transformation can be formulated as:

$$\{R^O_{(w,h)}, G^O_{(w,h)}, B^O_{(w,h)}, NIR^O_{(w,h)}\} = f_{AOLUT}(V^1_{(w,h)}, V^2_{(w,h)}, V^3_{(w,h)}, V^4_{(w,h)}, V^5_{(w,h)}), \quad (6)$$

where $f_{AOLUT}(\cdot)$ denotes the lookup and interpolation process in the LUT retrieval. More details about AOLUT and the pentalinear interpolation can be found in Section A.4.

3.5 Loss Function

To achieve satisfying pan-sharpening results, we propose a joint loss for network training. Suppose the batch size is T. We first utilize the MSE loss:

$$\mathcal{L}_{mse} = \frac{1}{T}\sum_{t=1}^{T} \|HRMS_t - GT_t\|^2, \quad (7)$$

where $HRMS$ and GT denote the network output and the corresponding ground truth, respectively.

To enhance the stability and robustness of the learned LUTs, we incorporate smoothness regularization $\mathcal{L}_s$ and monotonicity regularization $\mathcal{L}_m$:

$$\mathcal{L}_s = \mathcal{L}_s^{PG} + \mathcal{L}_s^{SD} + \mathcal{L}_s^{AO}, \mathcal{L}_m = \mathcal{L}_m^{PG} + \mathcal{L}_m^{SD} + \mathcal{L}_m^{AO}, \quad (8)$$

where $\mathcal{L}_s^{PG}$, $\mathcal{L}_s^{SD}$, and $\mathcal{L}_s^{AO}$ denote the smoothness regularizations for PGLUT, SDLUT, and AOLUT, while $\mathcal{L}_m^{PG}$, $\mathcal{L}_m^{SD}$, and $\mathcal{L}_m^{AO}$ represent the monotonicity regularizations for PGLUT, SDLUT, and AOLUT, respectively.

Taking SDLUT as an example, the smoothness regularization can be defined as:

$$\begin{aligned}\mathcal{L}_s^{SD} = \sum_{O\in\{l,o,c,a\}} \sum_{i,j,k,m=0}^{N-1} (&\left\|O_{(i+1,j,k,m)} - O_{(i,j,k,m)}\right\|^2 \\ &+ \left\|O_{(i,j+1,k,m)} - O_{(i,j,k,m)}\right\|^2 \\ &+ \left\|O_{(i,j,k+1,m)} - O_{(i,j,k,m)}\right\|^2 \\ &+ \left\|O_{(i,j,k,m+1)} - O_{(i,j,k,m)}\right\|^2),\end{aligned} \quad (9)$$

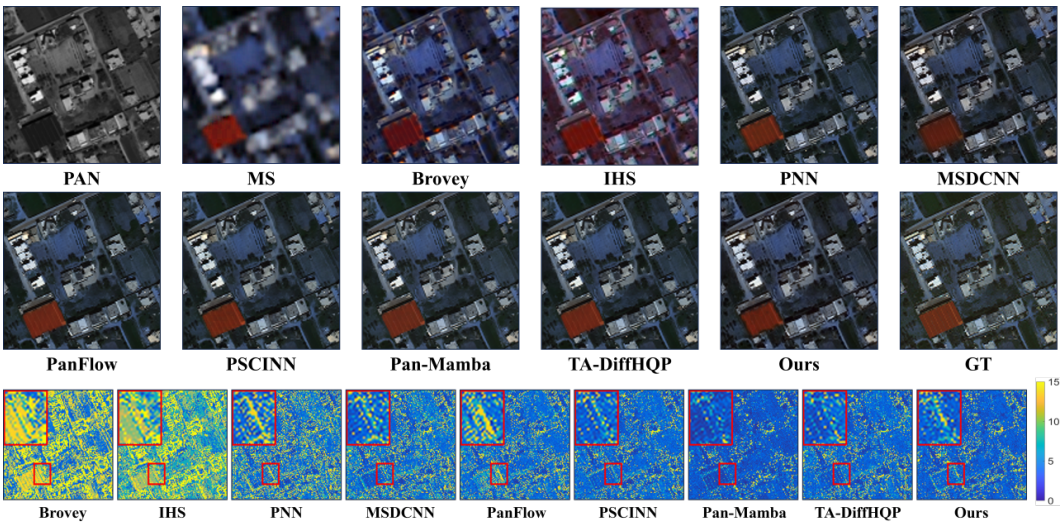

Figure 3: Visual comparison on WorldView-III dataset. The last row visualizes the MSE residues between the pan-sharpening results and the ground truth.

where N represents the number of bins in each dimension of the LUT. $O_{(i,j,k,m)}$ is the corresponding output for the defined sampling point (i, j, k, m) in LUT. The definitions of $\mathcal{L}s^{PG}$ and $\mathcal{L}s^{AO}$ are similar to those in Equation 36.

The monotonicity regularization in AOLUT can be defined as:

$$\begin{aligned}\mathcal{L}_m^{SD} = \sum_{O\in\{l,o,c,a\}} \sum_{i,j,k,m=0}^{N-1} [&g(O_{(i,j,k,m)} - O_{(i+1,j,k,m)}) \\ &+g(O_{(i,j,k,m)} - O_{(i,j+1,k,m)}) \\ &+g(O_{(i,j,k,m)} - O_{(i,j,k+1,m)}) \\ &+g(O_{(i,j,k,m)} - O_{(i,j,k,m+1)})],\end{aligned} \tag{10}$$

where $g(\cdot)$ denotes the ReLU activation function. Similarly, $\mathcal{L}_m^{PG}$ and $\mathcal{L}_m^{AO}$ are defined in the same way as in Equation 37.

The final loss functions are as follows:

$$\mathcal{L} = \mathcal{L}_1 + \lambda_s \mathcal{L}_s + \lambda_m \mathcal{L}_m, \tag{11}$$

where the two constant parameters λ_s and λ_m are used to control the effects of the smoothness and monotonicity regularization terms, respectively. In our experiments, we empirically set λ_s = 0.0001 and λ_m = 10. More details about the loss functions can be found in Section A.5

4 Experiments

4.1 Datasets

Remote sensing datasets from three satellites are used in our experiments, including WorldView-II (WV2), GaoFen2 (GF2) and WorldView-III (WV3). Due to the absence of high-resolution multispectral ground truth images in these datasets, we generate the training set using the Wald protocol tool [43]. Specifically, given the original MS image and its corresponding high-resolution PAN image, they are downsampled by a factor of r to obtain image pairs of MS and PAN, with r set to 4. During training, the original high-resolution MS image is treated as the ground truth, while the MS and PAN images serve as the input image pairs.

4.2 Implementation Details

We compare the proposed Pan-LUT model against several pan-sharpening methods on reduced-resolution scenes from WV2, WV3, and GF2 datasets. Specifically, we choose four traditional

Table 2: Evaluation on the real-world full-resolution scenes from WorldView-II dataset. The best values are highlighted by red. The up or down arrow indicates higher or lower metric corresponding to better results.

Metrics	Brovey	IHS	PNN	MSDCNN	GPPNN	SFDI	UCGAN	PanFlow	PSCINN	Pan-Mamba	TA-DiffHQP	Ours
$D_\lambda \downarrow$	0.1026	0.1110	0.1057	0.1063	0.0987	0.1034	0.1042	0.0966	0.0967	0.0966	0.0953	0.0571
$D_S \downarrow$	0.1409	0.1556	0.1446	0.1443	0.1312	0.1305	0.1476	0.1274	0.1271	0.1272	0.1129	0.0640
QNR↑	0.7728	0.7527	0.7684	0.7683	0.7859	0.7827	0.7650	0.7910	0.7904	0.7911	0.8025	0.8829

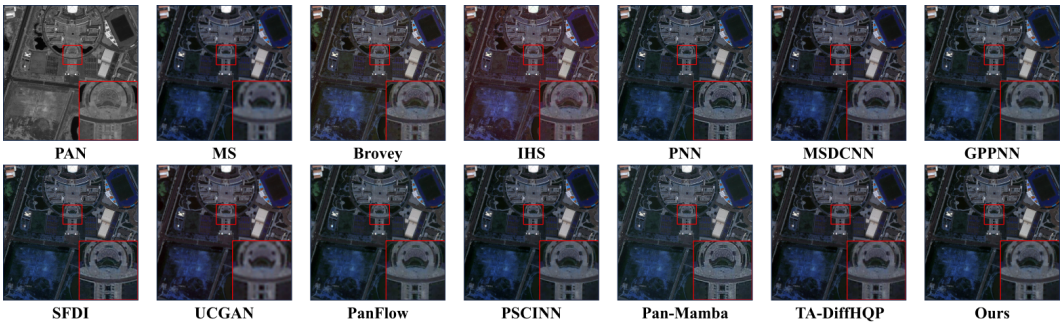

Figure 4: Visual comparison on the real full-resolution scenes from the WorldView-II dataset. For a more detailed examination of the results, we zoomed-in view on specific parts of the images.

pan-sharpening techniques: Brovey [14], IHS [4], SFIM [35] and GS [24], along with ten deep learning-based approaches: PNN [38], PanNet [56], MSDCNN [57], Pan-GAN [37], SFDI [67], UCGAN [65], PanFlow [55], PSCINN [44], Pan-Mamba [15] and TA-DiffHQP [48]. Several widely used image quality assessment metrics are employed to evaluate the performance of the algorithm, including peak signal-to-noise ratio (PSNR) [19], structural similarity index (SSIM) [51], spectral angle mapper (SAM) [58], relative dimensionless global error in synthesis (ERGAS) [42], spectral distortion index(D_λ), spatial distortion index (D_S) and the quality with no reference (QNR) [3]. The PyTorch framework is implemented in our experiment. During the training phase, we employ an ADAM optimizer with $\beta_1 = 0.9$ and $\beta_2 = 0.999$, to update the network parameters for 1000 epochs with a batch size of 1. The learning rate is initialized with 5×10^{-4}. In parallel, a StepLR learning rate adjustment strategy is employed to reduce the learning rate by half after every 200 iterations. The sizes of PGLUT, SDLUT and AOLUT are set to 9, 9 and 9, respectively.

4.3 Comparison with Other Methods

Evaluation on Reduced-resolution Scene. The quantitative results across three datasets are presented in Table 1, with the best results highlighted in red. Compared to traditional methods, Pan-LUT achieves an average PSNR improvement of 5dB, 7dB, and 7dB across the three datasets, while maintaining inference speeds comparable to those of traditional methods. It is worth noting that the proposed Pan-LUT does not incorporate any network structure, yet it outperforms some DNN-based methods, such as PanNet and PNN, in terms of both performance and inference time. We also provide visual comparisons for the WV3 datasets, as shown in Figure 3.

Evaluation on Full-resolution Scene. To assess the performance and generalization capability of our method on full-resolution scenes under real-world conditions, we first trained Pan-LUT on the reduced-resolution WorldView-II data and then tested it on unseen full-resolution WorldView-II satellite datasets. The real-world dataset consists of 200 newly collected samples from the WorldView-II satellite for evaluation. The results are presented in Table 2. On reduced-resolution scenes, our method falls short of most DNN-based approaches in terms of performance. However, on full-resolution scenes, it outperforms all of them when considering the metrics of D_λ, D_S, and QNR. This demonstrates its strong generalization ability in real-world situations. Additionally, we provide a visual comparison against both traditional and DNN-based methods, as shown in Figure 4.

Computation Efficiency Comparison. We conduct three experiments to comprehensively evaluate the computational efficiency of all methods: (1) testing the maximum image size that each method can handle on 11GB and 24GB GPUs; (2) measuring their inference time on the CPU; and (3) evaluating their inference time on an RTX 2080 Ti GPU with 2K×2K and 4K×4K images. For each method, we record the average inference time on 100 images. As shown in Figure 1, even

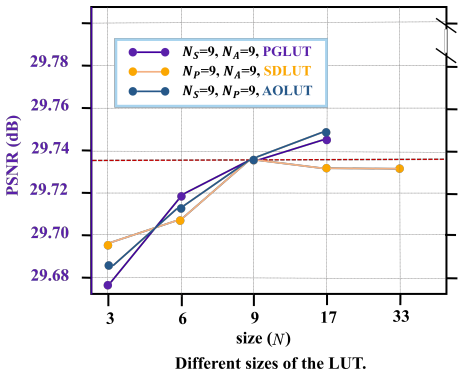

Figure 5: Ablation studies on different sizes of the PGLUT, SDLUT and AOLUT on the WorldView-III dataset.

Table 3: Memory requirements (K).

Module	3	6	9	17	33
AOLUT	0.97	31.10	236.20	5679.43	156541.57
SDLUT	0.08	1.30	6.56	83.52	1185.92
PGLUT	1.21	38.88	295.24	7099.28	195676.96

Table 4: Ablation study of PGLUT, SDLUT and AOLUT on the WorldView-III dataset.

Config	PSNR↑	SSIM↑	SAM↓	ERGAS↓
(i) only PGLUT	25.2788	0.7742	0.1130	5.4852
(ii) only SDLUT	26.1433	0.8165	0.1123	5.4211
(iii) only AOLUT	28.9554	0.8677	0.1001	3.7661
(iv) PGLUT and SDLUT	29.1315	0.8795	0.0988	3.6785
(v) SDLUT and AOLUT	29.2754	0.9010	0.0934	3.6033
(vi) PGLUT and AOLUT	29.4875	0.8925	0.0900	3.4977
⋆ **Pan-LUT (Ours)**	29.7376	0.9106	0.0815	3.3934

with a 24GB GPU, existing methods fail to process 8K×8K images, while our method can handle 9K×9K images on an 11GB GPU. In environments without GPU acceleration, most methods exhibit unsatisfactory inference speed. As shown in Tabel 1, Pan-LUT efficiently processes images at all resolutions. Compared to DNN-based methods, it achieves significantly faster inference speeds, while maintaining comparable speed to traditional methods. Our method easily meets the real-time processing requirements on GPUs, outperforming all other methods by a substantial margin. Notably, only PNN is capable of handling remote sensing satellite images at the 4K×4K resolution, highlighting the superior efficiency of our approach.

4.4 Ablation Study

Size of Look-Up Tables. As shown in Figure 5, changing the LUT size does not lead to a significant drop in performance. This observation suggests that the effectiveness of our proposed method is not dependent on consuming extensive storage resources to increase the LUT size. First, we examine the effect of PGLUT size, denoted N_P. Performance improves with larger N_P, reaching an optimal point at values N_P = 9. Beyond this (from 9 to 17), only a minor gain of 0.01 dB is observed, while the number of parameters increases substantially from 236K to 5M, indicating capacity redundancy. Therefore, we set N_P = 9 as the default to balance performance with storage requirements. For SDLUT, denoted N_S, increasing N_S from 3 to 9 improves performance, but values above 9 cause a slight performance drop. Similarly, enlarging the AOLUT size N_A yields only minor gains but substantially increases parameters, especially beyond N_A = 9. We thus set N_A = 9 to balance performance with computational efficiency. We provide the parameter count for each LUT of different sizes in Tabel 3, which can be calculated as follows:

$$Param_{PGLUT} = 5N^5, Param_{SDLUT} = N^4, Param_{AOLUT} = 4N^5. \tag{12}$$

Effectiveness of Each LUT. We further conduct ablation studies to verify the effectiveness of each LUT. Results are listed in Table 4. Our observations are as follows: 1) Comparing (i) with (iv) and (iii) with (v), SDLUT effectively captures fine-grained spatial details from the PAN image, thereby enhancing overall performance. 2) Comparing (ii) with (iv) and (iii) with (iv), PGLUT provides finer control over spectral transformation, resulting in improved performance. 3) Comparing (ii) with (v) and (i) with (vi), AOLUT demonstrates adaptive aggregation capabilities.

5 Conclusion

In this paper, we propose a novel learnable LUT framework, called Pan-LUT, which strikes an optimal balance between performance and computational efficiency for high-resolution remote sensing images in pan-sharpening. The proposed method makes it possible to process $15K \times 15K$ remote sensing images on a 24GB GPU and processes a 9K×9K image in under 1 ms using one RTX 2080 Ti GPU. Extensive experiments on various satellite datasets demonstrate the effectiveness and efficiency of Pan-LUT.

6 Acknowledgments

This work was supported in part by the National Natural Science Foundation of China under Grant 82172073 and Grant 62271430, and in part by the Open Fund of the National Key Laboratory of Infrared Detection Technologies.

References

[1] B. Aiazzi, L. Alparone, S. Baronti, A. Garzelli, and M. Selva. Mtf-tailored multiscale fusion of high-resolution ms and pan imagery. *Photogrammetric Engineering & Remote Sensing*, 72(5):591–596, 2006.

[2] B. Aiazzi, S. Baronti, and M. Selva. Improving component substitution pansharpening through multivariate regression of ms + pan data. *IEEE Transactions on Geoscience and Remote Sensing*, 45(10):3230–3239, 2007.

[3] L. Alparone, B. Aiazzi, S. Baronti, A. Garzelli, F. Nencini, and M. Selva. Multispectral and panchromatic data fusion assessment without reference. *Photogrammetric Engineering & Remote Sensing*, 74(2):193–200, 2008.

[4] W. Carper, T. Lillesand, R. Kiefer, et al. The use of intensity-hue-saturation transformations for merging spot panchromatic and multispectral image data. *Photogrammetric Engineering and remote sensing*, 56(4):459–467, 1990.

[5] P. Chavez and A. Kwarteng. Extracting spectral contrast in landsat thematic mapper image data using selective principal component analysis. *Photogrammetric Engineering and Remote Sensing,Photogrammetric Engineering and Remote Sensing*, Feb 1989.

[6] Y. Chen, H. Liu, and F. Fang. A novel pansharpening method based on cross stage partial network and transformer. *Scientific reports*, 14(1):12631, 2024.

[7] Z.-X. Chen, C. Jin, T.-J. Zhang, X. Wu, and L.-J. Deng. Spanconv: A new convolution via spanning kernel space for lightweight pansharpening. In *IJCAI*, pages 841–847, 2022.

[8] J. Choi, K. Yu, and Y. Kim. A new adaptive component-substitution-based satellite image fusion by using partial replacement. *IEEE transactions on geoscience and remote sensing*, 49(1):295–309, 2010.

[9] M. V. Conde, J. Vazquez-Corral, M. S. Brown, and R. Timofte. Nilut: Conditional neural implicit 3d lookup tables for image enhancement. In *Proceedings of the AAAI Conference on Artificial Intelligence*, volume 38, pages 1371–1379, 2024.

[10] F. DadrasJavan, F. Samadzadegan, and F. Fathollahi. Spectral and spatial quality assessment of ihs and wavelet based pan-sharpening techniques for high resolution satellite imagery. *Image Video Process*, 6(1), 2018.

[11] C. Dong, C. C. Loy, K. He, and X. Tang. Image super-resolution using deep convolutional networks. *IEEE transactions on pattern analysis and machine intelligence*, 38(2):295–307, 2015.

[12] Y. Duan, X. Wu, H. Deng, and L.-J. Deng. Content-adaptive non-local convolution for remote sensing pansharpening. In *Proceedings of the IEEE/CVF Conference on Computer Vision and Pattern Recognition*, pages 27738–27747, 2024.

[13] D. Fasbender, J. Radoux, and P. Bogaert. Bayesian data fusion for adaptable image pansharpening. *IEEE Transactions on Geoscience and Remote Sensing*, 46(6):1847–1857, 2008.

[14] A. R. Gillespie, A. B. Kahle, and R. E. Walker. Color enhancement of highly correlated images. ii. channel ratio and "chromaticity" transformation techniques. *Remote Sensing of Environment*, page 343–365, Jul 1987.

[15] X. He, K. Cao, J. Zhang, K. Yan, Y. Wang, R. Li, C. Xie, D. Hong, and M. Zhou. Pan-mamba: Effective pan-sharpening with state space model. *Information Fusion*, 115:102779, 2025.

[16] X. He, K. Yan, R. Li, C. Xie, J. Zhang, and M. Zhou. Pyramid dual domain injection network for pan-sharpening. In *Proceedings of the IEEE/CVF International Conference on Computer Vision (ICCV)*, pages 12908–12917, October 2023.

[17] X. He, K. Yan, R. Li, C. Xie, J. Zhang, and M. Zhou. Frequency-adaptive pan-sharpening with mixture of experts. In *Proceedings of the AAAI Conference on Artificial Intelligence*, volume 38, pages 2121–2129, 2024.

[18] J. Hou, Q. Cao, R. Ran, C. Liu, J. Li, and L.-j. Deng. Bidomain modeling paradigm for pansharpening. In *Proceedings of the 31st ACM International Conference on Multimedia*, pages 347–357, 2023.

[19] Q. Huynh-Thu and M. Ghanbari. Scope of validity of psnr in image/video quality assessment. *Electronics letters*, 44(13):800–801, 2008.

[20] Z.-R. Jin, T.-J. Zhang, T.-X. Jiang, G. Vivone, and L.-J. Deng. Lagconv: Local-context adaptive convolution kernels with global harmonic bias for pansharpening. In *Proceedings of the AAAI conference on artificial intelligence*, volume 36, pages 1113–1121, 2022.

[21] Y. Jo and S. Joo Kim. Practical single-image super-resolution using look-up table. In *2021 IEEE/CVF Conference on Computer Vision and Pattern Recognition (CVPR)*, Jun 2021.

[22] M. M. Khan, J. Chanussot, L. Condat, and A. Montanvert. Indusion: Fusion of multispectral and panchromatic images using the induction scaling technique. *IEEE Geoscience and Remote Sensing Letters*, 5(1):98–102, 2008.

[23] R. L. King and J. Wang. A wavelet based algorithm for pan sharpening landsat 7 imagery. In *IGARSS 2001. Scanning the Present and Resolving the Future. Proceedings. IEEE 2001 International Geoscience and Remote Sensing Symposium (Cat. No. 01CH37217)*, volume 2, pages 849–851. IEEE, 2001.

[24] C. A. Laben and B. V. Brower. Process for enhancing the spatial resolution of multispectral imagery using pan-sharpening, Jan. 4 2000. US Patent 6,011,875.

[25] J. Li, C. Chen, Z. Cheng, and Z. Xiong. Mulut: Cooperating multiple look-up tables for efficient image super-resolution. In *European conference on computer vision*, pages 238–256. Springer, 2022.

[26] W. Li, G. Wu, W. Wang, P. Ren, and X. Liu. Fastllve: Real-time low-light video enhancement with intensity-aware look-up table. In *Proceedings of the 31st ACM International Conference on Multimedia*, pages 8134–8144, 2023.

[27] W. Liao, X. Huang, F. Van Coillie, G. Thoonen, A. Pižurica, P. Scheunders, and W. Philips. Two-stage fusion of thermal hyperspectral and visible rgb image by pca and guided filter. In *2015 7th Workshop on Hyperspectral Image and Signal Processing: Evolution in Remote Sensing (WHISPERS)*, pages 1–4. Ieee, 2015.

[28] J. Lin, Y. Wu, Z. Wang, X. Liu, and Y. Guo. Pair-id: A dual modal framework for identity preserving image generation. *IEEE Signal Processing Letters*, 2024.

[29] J. Lin, G. Zhao, J. Xu, G. Wang, Z. Wang, A. Dantcheva, L. Du, and C. Chen. Difftv: Identity-preserved thermal-to-visible face translation via feature alignment and dual-stage conditions. In *Proceedings of the 32nd ACM International Conference on Multimedia*, pages 10930–10938, 2024.

[30] Y. Lin, Z. Fu, G. Meng, Y. Wang, Y. Dong, L. Fan, H. Yu, and X. Ding. Domain-irrelevant feature learning for generalizable pan-sharpening. In *Proceedings of the 31st ACM International Conference on Multimedia*, pages 3287–3296, 2023.

[31] Y. Lin, Z. Fu, K. Wen, T. Ye, S. Chen, G. Meng, Y. Wang, Y. Huang, X. Tu, and X. Ding. Unsupervised low-light image enhancement with lookup tables and diffusion priors. *arXiv preprint arXiv:2409.18899*, 2024.

[32] Y. Lin, Z. Lin, H. Chen, P. Pan, C. Li, S. Chen, K. Wen, Y. Jin, W. Li, and X. Ding. Jarvisir: Elevating autonomous driving perception with intelligent image restoration. In *Proceedings of the Computer Vision and Pattern Recognition Conference*, pages 22369–22380, 2025.

[33] Y. Lin, T. Ye, S. Chen, Z. Fu, Y. Wang, W. Chai, Z. Xing, L. Zhu, and X. Ding. Aglldiff: Guiding diffusion models towards unsupervised training-free real-world low-light image enhancement. *arXiv preprint arXiv:2407.14900*, 2024.

[34] G. Liu, Y. Ding, M. Li, M. Sun, X. Wen, and B. Wang. Reconstructed convolution module based look-up tables for efficient image super-resolution. In *Proceedings of the IEEE/CVF International Conference on Computer Vision*, pages 12217–12226, 2023.

[35] J. Liu. Smoothing filter-based intensity modulation: A spectral preserve image fusion technique for improving spatial details. *International Journal of remote sensing*, 21(18):3461–3472, 2000.

[36] C. Ma, J. Zhang, J. Zhou, and J. Lu. Learning series-parallel lookup tables for efficient image super-resolution. In *European Conference on Computer Vision*, pages 305–321. Springer, 2022.

[37] J. Ma, W. Yu, C. Chen, P. Liang, X. Guo, and J. Jiang. Pan-gan: An unsupervised pan-sharpening method for remote sensing image fusion. *Information Fusion*, 62:110–120, 2020.

[38] G. Masi, D. Cozzolino, L. Verdoliva, and G. Scarpa. Pansharpening by convolutional neural networks. *Remote Sensing*, 8(7):594, 2016.

[39] G. Meng, J. Huang, Y. Wang, Z. Fu, X. Ding, and Y. Huang. Progressive high-frequency reconstruction for pan-sharpening with implicit neural representation. In *Proceedings of the AAAI Conference on Artificial Intelligence*, volume 38, pages 4189–4197, 2024.

[40] X. Otazu, M. González-Audícana, O. Fors, and J. Núñez. Introduction of sensor spectral response into image fusion methods. application to wavelet-based methods. *IEEE Transactions on Geoscience and Remote Sensing*, 43(10):2376–2385, 2005.

[41] F. Palsson, J. R. Sveinsson, and M. O. Ulfarsson. A new pansharpening algorithm based on total variation. *IEEE Geoscience and Remote Sensing Letters*, 11(1):318–322, 2013.

[42] L. Wald. *Data fusion: definitions and architectures: fusion of images of different spatial resolutions*. Presses des MINES, 2002.

[43] L. Wald, T. Ranchin, and M. Mangolini. Fusion of satellite images of different spatial resolutions: Assessing the quality of resulting images. *Photogrammetric engineering and remote sensing*, 63(6):691–699, 1997.

[44] J. Wang, T. Lu, X. Huang, R. Zhang, and X. Feng. Pan-sharpening via conditional invertible neural network. *Information Fusion*, 101:101980, 2024.

[45] T. Wang, Y. Li, J. Peng, Y. Ma, X. Wang, F. Song, and Y. Yan. Real-time image enhancer via learnable spatial-aware 3d lookup tables. In *Proceedings of the IEEE/CVF International Conference on Computer Vision*, pages 2471–2480, 2021.

[46] Y. Wang, X. He, Y. Dong, Y. Lin, Y. Huang, and X. Ding. Cross-modality interaction network for pan-sharpening. *IEEE Transactions on Geoscience and Remote Sensing*, 62:1–16, 2024.

[47] Y. Wang, Y. Lin, X. He, H. Zheng, K. Yan, L. Fan, Y. Huang, and X. Ding. Learning diffusion high-quality priors for pan-sharpening: A two-stage approach with time-aware adapter fine-tuning. *IEEE Transactions on Geoscience and Remote Sensing*, 2025.

[48] Y. Wang, Y. Lin, X. He, H. Zheng, K. Yan, L. Fan, Y. Huang, and X. Ding. Learning diffusion high-quality priors for pan-sharpening: A two-stage approach with time-aware adapter fine-tuning. *IEEE Transactions on Geoscience and Remote Sensing*, 2025.

[49] Y. Wang, Y. Lin, G. Meng, Z. Fu, Y. Dong, L. Fan, H. Yu, X. Ding, and Y. Huang. Learning high-frequency feature enhancement and alignment for pan-sharpening. In *Proceedings of the 31st ACM International Conference on Multimedia*, pages 358–367, 2023.

[50] Y. Wang, H. Zheng, F. Li, Y. Lin, L. Fan, X. He, Y. Huang, and X. Ding. Towards generalizable pan-sharpening: Conditional flow-based learning guided by implicit high-frequency priors. *IEEE Transactions on Geoscience and Remote Sensing*, 2025.

[51] Z. Wang, A. C. Bovik, H. R. Sheikh, and E. P. Simoncelli. Image quality assessment: from error visibility to structural similarity. *IEEE transactions on image processing*, 13(4):600–612, 2004.

[52] S. Xu, J. Zhang, Z. Zhao, K. Sun, J. Liu, and C. Zhang. Deep gradient projection networks for pan-sharpening. In *Proceedings of the IEEE/CVF Conference on Computer Vision and Pattern Recognition*, pages 1366–1375, 2021.

[53] K. Yan, M. Zhou, J. Huang, F. Zhao, C. Xie, C. Li, and D. Hong. Panchromatic and multispectral image fusion via alternating reverse filtering network. *Advances in Neural Information Processing Systems*, 35:21988–22002, 2022.

[54] K. Yan, M. Zhou, L. Zhang, and C. Xie. Memory-augmented model-driven network for pansharpening. In *European Conference on Computer Vision*, pages 306–322. Springer, 2022.

[55] G. Yang, X. Cao, W. Xiao, M. Zhou, A. Liu, X. Chen, and D. Meng. Panflownet: A flow-based deep network for pan-sharpening. In *Proceedings of the IEEE/CVF International Conference on Computer Vision*, pages 16857–16867, 2023.

[56] J. Yang, X. Fu, Y. Hu, Y. Huang, X. Ding, and J. Paisley. Pannet: A deep network architecture for pan-sharpening. In *Proceedings of the IEEE international conference on computer vision*, pages 5449–5457, 2017.

[57] Q. Yuan, Y. Wei, X. Meng, H. Shen, and L. Zhang. A multiscale and multidepth convolutional neural network for remote sensing imagery pan-sharpening. *IEEE Journal of Selected Topics in Applied Earth Observations and Remote Sensing*, 11(3):978–989, 2018.

[58] R. H. Yuhas, A. F. Goetz, and J. W. Boardman. Discrimination among semi-arid landscape endmembers using the spectral angle mapper (sam) algorithm. In *JPL, Summaries of the Third Annual JPL Airborne Geoscience Workshop. Volume 1: AVIRIS Workshop*, 1992.

[59] H. Zeng, J. Cai, L. Li, Z. Cao, and L. Zhang. Learning image-adaptive 3d lookup tables for high performance photo enhancement in real-time. *IEEE Transactions on Pattern Analysis and Machine Intelligence*, page 1–1, Jan 2020.

[60] F. Zhang, K. Zhang, J. Sun, J. Wang, and L. Bruzzone. Drformer: Learning disentangled representation for pan-sharpening via mutual information-based transformer. *IEEE Transactions on Geoscience and Remote Sensing*, 62:1–15, 2023.

[61] C.-Y. Zhao, T.-J. Zhang, R. Ran, Z.-X. Chen, and L.-J. Deng. Lgpconv: Learnable gaussian perturbation convolution for lightweight pansharpening. In *IJCAI*, pages 4647–4655, 2023.

[62] K. Zheng, J. Huang, M. Zhou, D. Hong, and F. Zhao. Deep adaptive pansharpening via uncertainty-aware image fusion. *IEEE Transactions on Geoscience and Remote Sensing*, 61:1–15, 2023.

[63] Y. Zhong, X. Wu, L.-J. Deng, Z. Cao, and H.-X. Dou. Ssdiff: Spatial-spectral integrated diffusion model for remote sensing pansharpening. *Advances in Neural Information Processing Systems*, 37:77962–77986, 2025.

[64] H. Zhou, Q. Liu, and Y. Wang. Panformer: A transformer based model for pan-sharpening. In *2022 IEEE International Conference on Multimedia and Expo (ICME)*, pages 1–6. IEEE, 2022.

[65] H. Zhou, Q. Liu, D. Weng, and Y. Wang. Unsupervised cycle-consistent generative adversarial networks for pan sharpening. *IEEE Transactions on Geoscience and Remote Sensing*, 60:1–14, 2022.

[66] M. Zhou, J. Huang, Y. Fang, X. Fu, and A. Liu. Pan-sharpening with customized transformer and invertible neural network. In *Proceedings of the AAAI conference on artificial intelligence*, volume 36, pages 3553–3561, 2022.

[67] M. Zhou, J. Huang, K. Yan, H. Yu, X. Fu, A. Liu, X. Wei, and F. Zhao. Spatial-frequency domain information integration for pan-sharpening. In *European conference on computer vision*, pages 274–291. Springer, 2022.

[68] M. Zhou, K. Yan, X. Fu, A. Liu, and C. Xie. Pan-guided band-aware multi-spectral feature enhancement for pan-sharpening. *IEEE Transactions on Computational Imaging*, 9:238–249, 2023.

[69] Z. Zhu, X. Cao, M. Zhou, J. Huang, and D. Meng. Probability-based global cross-modal upsampling for pansharpening. In *Proceedings of the IEEE/CVF Conference on Computer Vision and Pattern Recognition*, pages 14039–14048, 2023.

A Appendix

The following contents are provided in the appendix:

- Limitation and Border Impact.
- More Technical Details.
- More ablation study.
- More comparison experiments.
- More visualization about our experiments.

A.1 Limitation and Border Impact

Limitation. One limitation of existing methods is the lack of neural network integration. While combining LUTs with neural structures may offer greater modeling capacity, it often comes at the cost of computational efficiency. Conversely, LUTs alone require substantial storage space, making them less suitable for high-dimensional input processing. The space complexity of an n-dimensional LUT is $O(ND^n)$, meaning its size increases exponentially with higher dimensions. This exponential growth severely limits its practical applicability, particularly when dealing with high-dimensional inputs. Lightweight network architectures must be further explored to facilitate efficient integration with LUTs. Meanwhile, more efficient LUT designs are essential for processing high-dimensional inputs.

A.2 Details of PGLUT

Input: Suppose that the MS image ($MS \in R^{H/r \times W/r \times C}$) and the PAN image ($P \in R^{H \times W \times 1}$) are given, the input of PGLUT ($I_{PG} \in R^{H \times W \times (C+1)}$) can be formulated as:

$$I_{PG} = Concat(P, MS \uparrow), \tag{13}$$

where $Concat(\cdot)$ is the concatenation operation. $MS \uparrow$ denotes the upsampled MS image. $MS \uparrow$ and P have the same spatial resolution.

Output: the output of PGLUT ($O_{PG} \in R^{H \times W \times (C+1)}$) can be formulated as:

$$O_{PG} = F_{PGLUT}(I_{PG}), \tag{14}$$

where $F_{PGLUT}(\cdot)$ denotes the lookup and pentalinear interpolation based on the PGLUT.

PAN-guided indexing strategy. In a MS image, pixels from different spatial locations may have identical values (e.g., $r_i = r_j, g_i = g_j, b_i = b_j, nir_i = nir_j$, where $i \neq j$). The LUT maps these identical inputs to the same output. The PAN-guided indexing strategy provides a more flexible indexing mechanism for the LUT. Specifically, it additionally considers the pixels at corresponding spatial positions in the PAN image (e.g., $r_i = r_j, g_i = g_j, b_i = b_j, nir_i = nir_j, pa_i \neq pa_j$, where $i \neq j$), thereby achieving finer-grained mapping. Given an input value $I_{(w,h)} = \{pa^I_{(w,h)}, r^I_{(w,h)}, g^I_{(w,h)}, b^I_{(w,h)}, nir^I_{(w,h)}\}$, where (w, h) denotes the spatial position of a pixel in the image, the input index to the PGLUT based on the input value can be represented as (x, y, z, s, e). PGLUT first performs a lookup operation to locate the nearest 32 adjacent elements around the input index in the PGLUT. We use (i, j, k, m, n) to denote the coordinates of a defined sampling point in PGLUT, which can be calculated as follows:

$$\begin{gathered} x = \frac{pa^I_{(w,h)}}{V_{max}} \cdot N, y = \frac{r^I_{(w,h)}}{V_{max}} \cdot N, z = \frac{g^I_{(w,h)}}{V_{max}} \cdot N, \\ s = \frac{b^I_{(w,h)}}{V_{max}} \cdot N, e = \frac{nir^I_{(w,h)}}{V_{max}} \cdot N, \\ i = \lfloor x \rfloor, j = \lfloor y \rfloor, k = \lfloor z \rfloor, m = \lfloor s \rfloor, n = \lfloor e \rfloor, \end{gathered} \tag{15}$$

where V_{max} denotes the maximum value (e.g., 255, 1023 or 2047). $\lfloor \cdot \rfloor$ denotes the floor function. Then, the offset between the input precise index (x, y, z, s, e) and the computed sampling point (i, j, k, m, n) can be computed:

$$\begin{gathered} d_x = x - i, d_y = y - j, d_z = z - k, \\ d_s = s - m, d_e = e - m, \\ d_{-x} = 1 - d_x, d_{-y} = 1 - d_y, d_{-z} = 1 - d_z, \\ d_{-s} = 1 - d_s, d_{-e} = 1 - d_e. \end{gathered} \tag{16}$$

Pentalinear Interpolation. After locating 32 adjacent points, an appropriate interpolation technique is applied to generate the output value using the values of these sampled points:

$$\begin{aligned}
O_{PG(x,y,z,s,e)} = {} & d_{-x}d_{-y}d_{-z}d_{-s}d_{-e}O_{(i,j,k,m,n)} + d_x d_{-y}d_{-z}d_{-s}d_{-e}O_{(i+1,j,k,m,n)} \\
& + d_{-x}d_y d_{-z}d_{-s}d_{-e}O_{(i,j+1,k,m,n)} + d_{-x}d_{-y}d_z d_{-s}d_{-e}O_{(i,j,k+1,m,n)} \\
& + d_{-x}d_{-y}d_{-z}d_s d_{-e}O_{(i,j,k,m+1,n)} + d_{-x}d_{-y}d_{-z}d_{-s}d_e O_{(i,j,k,m,n+1)} \\
& + d_x d_y d_{-z}d_{-s}d_{-e}O_{(i+1,j+1,k,m,n)} + d_x d_{-y}d_z d_{-s}d_{-e}O_{(i+1,j,k+1,m,n)} \\
& + d_x d_{-y}d_{-z}d_s d_{-e}O_{(i+1,j,k,m+1,n)} + d_x d_{-y}d_{-z}d_{-s}d_e O_{(i+1,j,k,m,n+1)} \\
& + d_{-x}d_y d_z d_{-s}d_{-e}O_{(i,j+1,k+1,m,n)} + d_{-x}d_y d_{-z}d_s d_{-e}O_{(i,j+1,k,m+1,n)} \\
& + d_{-x}d_y d_{-z}d_{-s}d_e O_{(i,j+1,k,m,n+1)} + d_{-x}d_{-y}d_z d_s d_{-e}O_{(i,j,k+1,m+1,n)} \\
& + d_{-x}d_{-y}d_z d_{-s}d_e O_{(i,j,k+1,m,n+1)} + d_{-x}d_{-y}d_{-z}d_s d_e O_{(i,j,k,m+1,n+1)} \\
& + d_x d_y d_z d_{-s}d_{-e}O_{(i+1,j+1,k+1,m,n)} + d_x d_y d_{-z}d_s d_{-e}O_{(i+1,j+1,k,m+1,n)} \\
& + d_x d_y d_{-z}d_{-s}d_e O_{(i+1,j+1,k,m,n+1)} + d_x d_{-y}d_z d_s d_{-e}O_{(i+1,j,k+1,m+1,n)} \\
& + d_x d_{-y}d_z d_{-s}d_e O_{(i+1,j,k+1,m,n+1)} + d_x d_{-y}d_{-z}d_s d_e O_{(i+1,j,k,m+1,n+1)} \\
& + d_{-x}d_y d_z d_s d_{-e}O_{(i,j+1,k+1,m+1,n)} + d_{-x}d_y d_z d_{-s}d_e O_{(i,j+1,k+1,m,n+1)} \\
& + d_{-x}d_y d_{-z}d_s d_e O_{(i,j+1,k,m+1,n+1)} + d_{-x}d_{-y}d_z d_s d_e O_{(i,j,k+1,m+1,n+1)} \\
& + d_x d_y d_z d_s d_{-e}O_{(i+1,j+1,k+1,m+1,n)} + d_x d_y d_z d_{-s}d_e O_{(i+1,j+1,k+1,m,n+1)} \\
& + d_x d_y d_{-z}d_s d_e O_{(i+1,j+1,k,m+1,n+1)} + d_x d_{-y}d_z d_s d_e O_{(i+1,j,k+1,m+1,n+1)} \\
& + d_{-x}d_y d_z d_s d_e O_{(i,j+1,k+1,m+1,n+1)} + d_x d_y d_z d_s d_e O_{(i+1,j+1,k+1,m+1,n+1)},
\end{aligned} \tag{17}$$

where $O_{(i,j,k,m,n)}$ represents the value of the LUT at the coordinate (i, j, k, m, n).

A.3 Details of SDLUT

Input: The input image ($O_{PG} \in R^{H\times W\times(C+1)}$) of SDLUT is the output of PGLUT.

Output: The output of SDLUT ($O_{SD} \in R^{H\times W\times(C+1)}$) can be formulated as:

$$O_{SD} = F_{SDLUT}(O_{PG}), \tag{18}$$

where $F_{SDLUT}(\cdot)$ denotes the lookup and quadrilinear interpolation based on the SDLUT.

Look Up. Specifically, for each channel of input, SDLUT operates by iterating through pixels one at a time, treating each as the current pixel during processing. Given the input current pixel and ajacent pixels, which denoted as $p_{(w,h)}$, $p_{(w+1,h)}$, $p_{(w,h+1)}$ and $p_{(w+1,h+1)}$ respectively, the input index to the SDLUT based on the input can be represented as (x, y, z, s). SDLUT first performs a lookup operation to locate the nearest 16 adjacent elements around the input index in the SDLUT. We use (i, j, k, m) to denote the coordinates of a defined sampling point in PGLUT, which can be calculated as follows:

$$\begin{aligned}
x = \frac{p_{(w,h)}}{V_{max}} \cdot N, y = \frac{p_{(w+1,h)}}{V_{max}} \cdot N, \\
z = \frac{p_{(w,h+1)}}{V_{max}} \cdot N, s = \frac{p_{(w+1,h+1)}}{V_{max}} \cdot N, \\
i = \lfloor x \rfloor, j = \lfloor y \rfloor, k = \lfloor z \rfloor, m = \lfloor s \rfloor,
\end{aligned} \tag{19}$$

where V_{max} denotes the maximum pixel value. $\lfloor \cdot \rfloor$ signifies the floor function. Then, the offset between the input precise index (x, y, z, s) and the computed sampling point (i, j, k, m) can be computed:

$$\begin{aligned}
d_x = x - i, d_y = y - j, d_z = z - k, d_s = s - m, \\
d_{-x} = 1 - d_x, d_{-y} = 1 - d_y, \\
d_{-z} = 1 - d_z, d_{-s} = 1 - d_s.
\end{aligned} \tag{20}$$

Quadrilinear Interpolation. After locating 16 adjacent points, an appropriate interpolation technique is applied to generate the output value using the values of these sampled points:

$$\begin{aligned}
O_{SD(x,y,z,s)} = {} & d_{-x}d_{-y}d_{-z}d_{-s}O_{(i,j,k,m)} + d_x d_{-y}d_{-z}d_{-s}O_{(i+1,j,k,m)} \\
& + d_{-x}d_y d_{-z}d_{-s}O_{(i,j+1,k,m)} + d_{-x}d_{-y}d_z d_{-s}O_{(i,j,k+1,m)} \\
& + d_{-x}d_{-y}d_{-z}d_s O_{(i,j,k,m+1)} + d_x d_y d_{-z}d_{-s}O_{(i+1,j+1,k,m)} \\
& + d_x d_{-y}d_z d_{-s}O_{(i+1,j,k+1,m)} + d_x d_{-y}d_{-z}d_s O_{(i+1,j,k,m+1)} \\
& + d_{-x}d_y d_z d_{-s}O_{(i,j+1,k+1,m)} + d_{-x}d_y d_{-z}d_s O_{(i,j+1,k,m+1)} \\
& + d_{-x}d_{-y}d_z d_s O_{(i,j,k+1,m+1)} + d_x d_y d_z d_{-s}O_{(i+1,j+1,k+1,m)} \\
& + d_x d_y d_{-z}d_s O_{(i+1,j+1,k,m+1)} + d_x d_{-y}d_z d_s O_{(i+1,j,k+1,m+1)} \\
& + d_{-x}d_y d_z d_s O_{(i,j+1,k+1,m+1)} + d_x d_y d_z d_s O_{(i+1,j+1,k+1,m+1)},
\end{aligned} \tag{21}$$

where $O_{(i,j,k,m)}$ represents the value of the LUT at the coordinate (i, j, k, m).

Rotation-indexing strategy. In general, the performance of the SDLUT can be improved when more pixels are considered. In order to exploit more area in the image, we use a Rotation-indexing strategy in the training phase. For our SDLUT, 4 rotational ensemble with 0, 90, 180, and 270 degrees covers total 3×3 pixels. Each output from the 4 rotations is defined as follow:

$$\begin{aligned} p^1_{(w,h)} &= F_{SDLUT}(p_{(w,h)}, p_{(w+1,h)}, p_{(w,h+1)}, p_{(w+1,h+1)}), \\ p^2_{(w,h)} &= F_{SDLUT}(p^1_{(w,h)}, p^1_{(w+1,h)}, p^1_{(w+1,h-1)}, p^1_{(w,h-1)}), \\ p^3_{(w,h)} &= F_{SDLUT}(p^2_{(w,h)}, p^2_{(w+1,h)}, p^2_{(w,h+1)}, p^2_{(w+1,h+1)}), \\ O_{SD(w,h)} &= F_{SDLUT}(p^3_{(w,h)}, p^3_{(w+1,h)}, p^3_{(w,h+1)}, p^3_{(w+1,h+1)}), \end{aligned} \tag{22}$$

where $F_{SDLUT}(\cdot)$ denotes the lookup and quadrilinear interpolation based on the SDLUT.

Proof Let (w, h) denote the pixel located at the w-th column and h-th row of the image. We provide a theoretical proof that Rotation-indexing strategy (RiS) extends the receptive field from 2×2 to 3×3. Ideally, we aim to incorporate all pixels within the local 3×3 region centered at (w, h), corresponding to the input index set:

$$\begin{aligned} G_{tgt} = \{&(w-1, h-1), (w, h-1), (w+1, h-1), (w-1, h), \\ &(w, h), (w+1, h), (w-1, h+1), (w, h+1), (w+1, h+1)\}. \end{aligned} \tag{23}$$

By default, SDLUT captures the bottom-right neighborhood of each pixel, with the corresponding input index group defined as:

$$G_{r0} = \{(w, h), (w+1, h), (w, h+1), (w+1, h+1)\}. \tag{24}$$

With the proposed RiS, SDLUT is applied to three rotated versions of the input, thereby effectively capturing a broader set of pixel neighborhoods.

$$\begin{aligned} G_{r90} &= \{(w, h), (w-1, h), (w, h+1), (w-1, h+1)\}, \\ G_{r180} &= \{(w, h), (w-1, h), (w, h-1), (w-1, h-1)\}, \\ G_{r270} &= \{(w, h), (w+1, h), (w, h-1), (w+1, h-1)\}. \end{aligned} \tag{25}$$

Then, we can derive the following equation:

$$G_{r0} \cup G_{r90} \cup G_{r180} \cup G_{r270} = G_{tgt}. \tag{26}$$

A.4 Details of AOLUT

Input: The input of AOLUT is the output from the SDLUT ($O_{SD} \in R^{H \times W \times (C+1)}$).

Output: the output of AOLUT ($O_{AO} \in R^{H \times W \times C}$) can be formulated as:

$$O_{AO} = F_{AOLUT}(O_{SD}), \tag{27}$$

where $F_{AOLUT}(\cdot)$ denotes the lookup and pentalinear interpolation based on the AOLUT.

Given an input value $I_{(w,h)} = \{O^{c_1}_{SD(w,h)}, O^{c_2}_{SD(w,h)}, O^{c_3}_{SD(w,h)}, O^{c_4}_{SD(w,h)}, O^{c_5}_{SD(w,h)}\}$, where (w, h) denotes the spatial position of a pixel in the image, $\{c_1, c_2, c_3, c_4, c_5\}$ denote the different channels of O_{SD}. The input index to the PGLUT based on the input value can be represented as (x, y, z, s, e). PGLUT first performs a lookup operation to locate the nearest 32 adjacent elements around the input index in the PGLUT. We use (i, j, k, m, n) to denote the coordinates of a defined sampling point in PGLUT, which can be calculated as follows:

$$\begin{aligned} x = \frac{O^{c_1}_{SD(w,h)}}{V_{max}} \cdot N, y = \frac{O^{c_2}_{SD(w,h)}}{V_{max}} \cdot N, z = \frac{O^{c_3}_{SD(w,h)}}{V_{max}} \cdot N, \\ s = \frac{O^{c_4}_{SD(w,h)}}{V_{max}} \cdot N, e = \frac{O^{c_5}_{SD(w,h)}}{V_{max}} \cdot N, \\ i = \lfloor x \rfloor, j = \lfloor y \rfloor, k = \lfloor z \rfloor, m = \lfloor s \rfloor, n = \lfloor e \rfloor, \end{aligned} \tag{28}$$

where V_{max} denotes the maximum value (e.g., 255, 1023 or 2047). $\lfloor \cdot \rfloor$ denotes the floor function. Then, the offset between the input precise index (x, y, z, s, e) and the computed sampling point (i, j, k, m, n) can be computed:

$$\begin{aligned} d_x = x - i, d_y = y - j, d_z = z - k, \\ d_s = s - m, d_e = e - m, \\ d_{-x} = 1 - d_x, d_{-y} = 1 - d_y, d_{-z} = 1 - d_z, \\ d_{-s} = 1 - d_s, d_{-e} = 1 - d_e. \end{aligned} \tag{29}$$

Pentalinear Interpolation. After locating 32 adjacent points, an appropriate interpolation technique is applied to generate the output value using the values of these sampled points:

$$\begin{aligned}
O_{AO(x,y,z,s,e)} = {} & d_{-x}d_{-y}d_{-z}d_{-s}d_{-e}O_{(i,j,k,m,n)} + d_x d_{-y}d_{-z}d_{-s}d_{-e}O_{(i+1,j,k,m,n)} \\
& + d_{-x}d_y d_{-z}d_{-s}d_{-e}O_{(i,j+1,k,m,n)} + d_{-x}d_{-y}d_z d_{-s}d_{-e}O_{(i,j,k+1,m,n)} \\
& + d_{-x}d_{-y}d_{-z}d_s d_{-e}O_{(i,j,k,m+1,n)} + d_{-x}d_{-y}d_{-z}d_{-s}d_e O_{(i,j,k,m,n+1)} \\
& + d_x d_y d_{-z}d_{-s}d_{-e}O_{(i+1,j+1,k,m,n)} + d_x d_{-y}d_z d_{-s}d_{-e}O_{(i+1,j,k+1,m,n)} \\
& + d_x d_{-y}d_{-z}d_s d_{-e}O_{(i+1,j,k,m+1,n)} + d_x d_{-y}d_{-z}d_{-s}d_e O_{(i+1,j,k,m,n+1)} \\
& + d_{-x}d_y d_z d_{-s}d_{-e}O_{(i,j+1,k+1,m,n)} + d_{-x}d_y d_{-z}d_s d_{-e}O_{(i,j+1,k,m+1,n)} \\
& + d_{-x}d_y d_{-z}d_{-s}d_e O_{(i,j+1,k,m,n+1)} + d_{-x}d_{-y}d_z d_s d_{-e}O_{(i,j,k+1,m+1,n)} \\
& + d_{-x}d_{-y}d_z d_{-s}d_e O_{(i,j,k+1,m,n+1)} + d_{-x}d_{-y}d_{-z}d_s d_e O_{(i,j,k,m+1,n+1)} \\
& + d_x d_y d_z d_{-s}d_{-e}O_{(i+1,j+1,k+1,m,n)} + d_x d_y d_{-z}d_s d_{-e}O_{(i+1,j+1,k,m+1,n)} \\
& + d_x d_y d_{-z}d_{-s}d_e O_{(i+1,j+1,k,m,n+1)} + d_x d_{-y}d_z d_s d_{-e}O_{(i+1,j,k+1,m+1,n)} \\
& + d_x d_{-y}d_z d_{-s}d_e O_{(i+1,j,k+1,m,n+1)} + d_x d_{-y}d_{-z}d_s d_e O_{(i+1,j,k,m+1,n+1)} \\
& + d_{-x}d_y d_z d_s d_{-e}O_{(i,j+1,k+1,m+1,n)} + d_{-x}d_y d_z d_{-s}d_e O_{(i,j+1,k+1,m,n+1)} \\
& + d_{-x}d_y d_{-z}d_s d_e O_{(i,j+1,k,m+1,n+1)} + d_{-x}d_{-y}d_z d_s d_e O_{(i,j,k+1,m+1,n+1)} \\
& + d_x d_y d_z d_s d_{-e}O_{(i+1,j+1,k+1,m+1,n)} + d_x d_y d_z d_{-s}d_e O_{(i+1,j+1,k+1,m,n+1)} \\
& + d_x d_y d_{-z}d_s d_e O_{(i+1,j+1,k,m+1,n+1)} + d_x d_{-y}d_z d_s d_e O_{(i+1,j,k+1,m+1,n+1)} \\
& + d_{-x}d_y d_z d_s d_e O_{(i,j+1,k+1,m+1,n+1)} + d_x d_y d_z d_s d_e O_{(i+1,j+1,k+1,m+1,n+1)},
\end{aligned} \tag{30}$$

where $O_{(i,j,k,m,n)}$ represents the value of the LUT at the coordinate (i, j, k, m, n).

A.5 Details of Loss Function

To achieve satisfying pan-sharpening results, we propose a joint loss for network training. Suppose the batch size is T. We first utilize the $\mathcal{L}_1$ loss:

$$\mathcal{L}_{mse} = \frac{1}{T}\sum_{t=1}^{T} \|HRMS_t - GT_t\|^2, \tag{31}$$

where $HRMS$ and GT denote the network output and the corresponding ground truth, respectively.

To enhance the stability and robustness of the learned LUTs, we incorporate smoothness regularization $\mathcal{L}_s$ and monotonicity regularization $\mathcal{L}_m$:

$$\mathcal{L}_s = \mathcal{L}_s^{PG} + \mathcal{L}_s^{SD} + \mathcal{L}_s^{AO}, \tag{32}$$

$$\mathcal{L}_m = \mathcal{L}_m^{PG} + \mathcal{L}_m^{SD} + \mathcal{L}_m^{AO}, \tag{33}$$

where $\mathcal{L}_s^{PG}$, $\mathcal{L}_s^{SD}$, and $\mathcal{L}_s^{AO}$ denote the smoothness regularizations for PGLUT, SDLUT, and AOLUT, while $\mathcal{L}_m^{PG}$, $\mathcal{L}_m^{SD}$, and $\mathcal{L}_m^{AO}$ represent the monotonicity regularizations for PGLUT, SDLUT, and AOLUT, respectively.

The Smoothness Regularization of PGLUT and AOLUT:

$$\begin{aligned}
\mathcal{L}_s^{PG}, \mathcal{L}_s^{AO} = \sum_{O\in\{l,o,c,a,e\}} \sum_{i,j,k,m,n=0}^{N-1} (& \left\| O_{(i+1,j,k,m,n)} \right. \\
& \left. - O_{(i,j,k,m,n)} \right\|^2 + \left\| O_{(i,j+1,k,m,n)} - O_{(i,j,k,m,n)} \right\|^2 \\
& + \left\| O_{(i,j,k+1,m,n)} - O_{(i,j,k,m,n)} \right\|^2 \\
& + \left\| O_{(i,j,k,m+1,n)} - O_{(i,j,k,m,n)} \right\|^2 \\
& + \left\| O_{(i,j,k,m,n+1)} - O_{(i,j,k,m,n)} \right\|^2).
\end{aligned} \tag{34}$$

The Monotonicity Regularization of PGLUT and AOLUT:

$$\begin{aligned}
\mathcal{L}_m^{PG}, \mathcal{L}_m^{AO} = \sum_{O\in\{l,o,c,a,e\}} \sum_{i,j,k,m,n=0}^{N-1} & [g(O_{(i,j,k,m,n)} \\
& - O_{(i+1,j,k,m,n)}) + g(O_{(i,j,k,m,n)} - O_{(i,j+1,k,m,n)}) \\
& + g(O_{(i,j,k,m,n)} - O_{(i,j,k+1,m,n)}) \\
& + g(O_{(i,j,k,m,n)} - O_{(i,j,k,m+1,n)}) \\
& + g(O_{(i,j,k,m,n)} - O_{(i,j,k,m,n+1)})],
\end{aligned} \tag{35}$$

Table 5: Ablation study on λ_m

Metrics	0	0.1	1	10	100
PSNR	29.5321	29.5421	29.6241	**29.7376**	29.4112

Table 6: Ablation study on λ_s

Metrics	0	0.00001	0.0001	0.001	0.01
PSNR	29.4746	29.4889	**29.7376**	29.5423	29.5213

where N represents the number of bins in each dimension of the LUT. $O_{(i,j,k,m,n)}$ is the corresponding output for the defined sampling point (i, j, k, m, n) in LUT. $g(\cdot)$ denotes the ReLU activation function.

The Smoothness Regularization of SDLUT:

$$\begin{aligned}\mathcal{L}_s^{SD} = \sum_{O\in\{l,o,c,a\}} \sum_{i,j,k,m=0}^{N-1} (\big\|O_{(i+1,j,k,m)} \\ -O_{(i,j,k,m)}\big\|^2 + \big\|O_{(i,j+1,k,m)} - O_{(i,j,k,m)}\big\|^2 \\ + \big\|O_{(i,j,k+1,m)} - O_{(i,j,k,m)}\big\|^2 \\ + \big\|O_{(i,j,k,m+1)} - O_{(i,j,k,m)}\big\|^2),\end{aligned} \tag{36}$$

The Monotonicity Regularization of SDLUT:

$$\begin{aligned}\mathcal{L}_m^{SD} = \sum_{O\in\{l,o,c,a\}} \sum_{i,j,k,m=0}^{N-1} [g(O_{(i,j,k,m)} \\ -O_{(i+1,j,k,m)}) + g(O_{(i,j,k,m)} - O_{(i,j+1,k,m)}) \\ +g(O_{(i,j,k,m)} - O_{(i,j,k+1,m)}) \\ +g(O_{(i,j,k,m)} - O_{(i,j,k,m+1)})],\end{aligned} \tag{37}$$

where N represents the number of bins in each dimension of the LUT. $O_{(i,j,k,m)}$ is the corresponding output for the defined sampling point (i, j, k, m) in LUT. $g(\cdot)$ denotes the ReLU activation function.

The final loss function is as follows:

$$\mathcal{L} = \mathcal{L}_1 + \lambda_s \mathcal{L}_s + \lambda_m \mathcal{L}_m, \tag{38}$$

where the two constant parameters λ_s and λ_m are used to control the effects of the smoothness and monotonicity regularization terms, respectively. In our experiments, we empirically set λ_s = 0.0001 and λ_m = 10.

A.6 Selection of regularization parameters.

As shown in Table 5, 6, we vary the λ_s and λ_m to determine the optimal parameters ($\lambda_m = 10$ and $\lambda_s = 0.0001$). A large λ_s (e.g., > 0.0001) results in worse PSNR, as the smooth regularization limits the flexibility of LUT transformations. In contrast, the PSNR is insensitive to the choice of λ_m since monotonicity is a natural constraint to LUTs.

A.7 More Comparison With Traditional methods

We further compare our method with additional traditional approaches, as shown in Table 7. While significantly surpassing traditional methods in performance across the three datasets, our approach maintains a comparable processing speed, highlighting its practical efficiency. Notably, some traditional methods are not only time-consuming but also inefficient.

A.8 More Visualization about Experiments

As shown in Figure 6 and Figure 7, extensive visual comparisons are provided for the WV2 and GF2 datasets. More visual comparisons are provided in the supplementary material.

Table 7: Quantitative comparison across three satellite datasets with traditional methods. The best outcomes are highlighted in red. ↑ indicates better performance with increasing values, while ↓ signifies improved performance with decreasing values.

Method	WorldView-II				GaoFen2				Worldview-III				Inference (ms)	
	PSNR↑	SSIM↑	SAM↓	ERGAS↓	PSNR↑	SSIM↑	SAM↓	ERGAS↓	PSNR↑	SSIM↑	SAM↓	ERGAS↓	2048×2048	4096×4096
PCA [5]	20.3542	0.7002	0.3741	10.8524	19.2933	0.7974	0.3908	14.3228	20.4455	0.5263	0.2693	10.3129	0.21	0.23
Brovey [14]	35.8646	0.9216	0.0403	1.8238	37.7974	0.9026	0.0218	1.3720	22.5060	0.5466	0.1159	8.2331	0.28	0.33
IHS [4]	35.2962	0.9027	0.0461	2.0278	38.1754	0.9100	0.0243	1.5336	22.5579	0.5354	0.1266	8.3616	0.23	0.26
SFIM [35]	34.1297	0.8975	0.0439	2.3449	36.9060	0.8882	0.0318	1.7398	21.8212	0.5457	0.1208	8.9730	0.32	0.47
Wavelet [23]	34.9827	0.8806	0.0481	2.0907	35.7502	0.8213	0.0283	2.0148	21.8551	0.5216	0.1368	9.1158	13.37	21.73
GS [24]	35.6376	0.9176	0.0423	1.8774	37.2260	0.9034	0.0309	1.6736	22.5608	0.5470	0.1217	8.2433	0.75	0.87
GSA [2]	35.3574	0.9219	0.097	1.7401	35.948	0.8779	0.0368	1.9257	21.8845	0.5458	0.1394	9.0781	0.73	0.76
GFPCA [27]	34.5580	0.9038	0.0488	2.1400	37.9443	0.9204	0.0314	1.5604	22.3344	0.4826	0.1294	8.3964	0.42	0.66
PRACS [8]	34.9671	0.9063	0.0414	1.8725	36.2015	0.8902	0.0372	1.8312	22.4452	0.5535	0.1373	8.2961	2.44	4.75
AWLP [40]	32.2402	0.8709	0.0457	2.4077	37.2183	0.8917	0.0281	1.5966	21.5792	0.5323	0.1260	9.0636	8.39	14.17
MTF-GLP-HPM [1]	31.3946	0.8722	0.0492	3.3040	37.9443	0.9204	0.0314	1.5604	21.1033	0.5505	0.1233	9.8406	4.22	6.09
Pan-LUT (**Ours**)	40.8555	0.9633	0.0254	1.0339	43.7466	0.9726	0.0169	0.8027	29.7376	0.9106	0.0815	3.3934	0.38	0.54

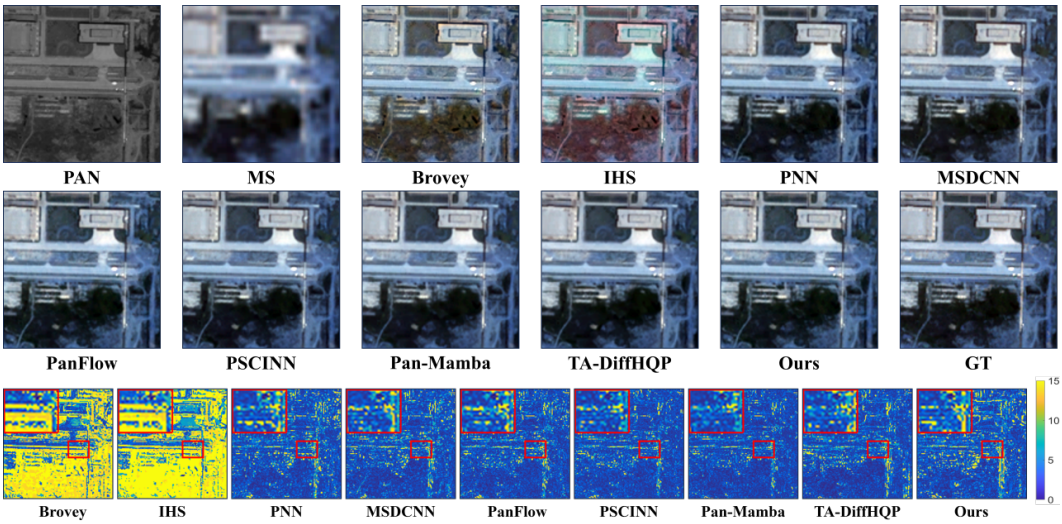

Figure 6: Visual comparison on WV2 dataset. The last row visualizes the MSE residues between the pan-sharpening results and the ground truth.

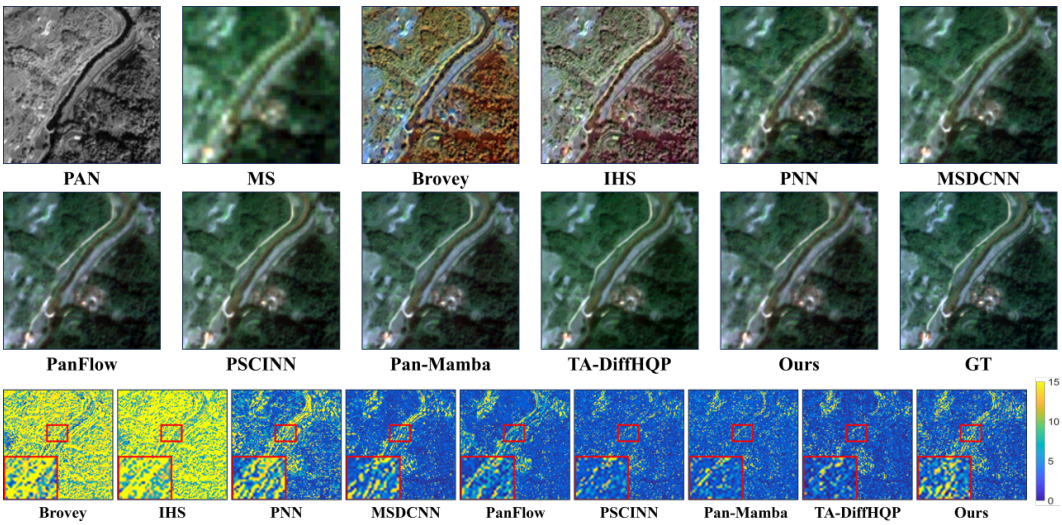

Figure 7: Visual comparison on GaoFen2 dataset. The last row visualizes the MSE residues between the pan-sharpening results and the ground truth.

NeurIPS Paper Checklist

1. **Claims**

   Question: Do the main claims made in the abstract and introduction accurately reflect the paper's contributions and scope?

   Answer: [Yes]

   Justification: The abstract and introduction sections offer a comprehensive discussion of the manuscript's context, intuition, and ambitions, as well as its contributions.

   Guidelines:

   - The answer NA means that the abstract and introduction do not include the claims made in the paper.
   - The abstract and/or introduction should clearly state the claims made, including the contributions made in the paper and important assumptions and limitations. A No or NA answer to this question will not be perceived well by the reviewers.
   - The claims made should match theoretical and experimental results, and reflect how much the results can be expected to generalize to other settings.
   - It is fine to include aspirational goals as motivation as long as it is clear that these goals are not attained by the paper.

2. **Limitations**

   Question: Does the paper discuss the limitations of the work performed by the authors?

   Answer: [Yes]

   Justification: The limitations of the work are discussed by authors in the Appendix.

   Guidelines:

   - The answer NA means that the paper has no limitation while the answer No means that the paper has limitations, but those are not discussed in the paper.
   - The authors are encouraged to create a separate "Limitations" section in their paper.
   - The paper should point out any strong assumptions and how robust the results are to violations of these assumptions (e.g., independence assumptions, noiseless settings, model well-specification, asymptotic approximations only holding locally). The authors should reflect on how these assumptions might be violated in practice and what the implications would be.
   - The authors should reflect on the scope of the claims made, e.g., if the approach was only tested on a few datasets or with a few runs. In general, empirical results often depend on implicit assumptions, which should be articulated.
   - The authors should reflect on the factors that influence the performance of the approach. For example, a facial recognition algorithm may perform poorly when image resolution is low or images are taken in low lighting. Or a speech-to-text system might not be used reliably to provide closed captions for online lectures because it fails to handle technical jargon.
   - The authors should discuss the computational efficiency of the proposed algorithms and how they scale with dataset size.
   - If applicable, the authors should discuss possible limitations of their approach to address problems of privacy and fairness.
   - While the authors might fear that complete honesty about limitations might be used by reviewers as grounds for rejection, a worse outcome might be that reviewers discover limitations that aren't acknowledged in the paper. The authors should use their best judgment and recognize that individual actions in favor of transparency play an important role in developing norms that preserve the integrity of the community. Reviewers will be specifically instructed to not penalize honesty concerning limitations.

3. **Theory assumptions and proofs**

   Question: For each theoretical result, does the paper provide the full set of assumptions and a complete (and correct) proof?

   Answer: [Yes]

   Justification: For each theoretical result, the paper provides the full set of assumptions and a complete (and correct) proof.

   Guidelines:

   - The answer NA means that the paper does not include theoretical results.
   - All the theorems, formulas, and proofs in the paper should be numbered and cross-referenced.

- All assumptions should be clearly stated or referenced in the statement of any theorems.
- The proofs can either appear in the main paper or the supplemental material, but if they appear in the supplemental material, the authors are encouraged to provide a short proof sketch to provide intuition.
- Inversely, any informal proof provided in the core of the paper should be complemented by formal proofs provided in appendix or supplemental material.
- Theorems and Lemmas that the proof relies upon should be properly referenced.

4. **Experimental result reproducibility**

   Question: Does the paper fully disclose all the information needed to reproduce the main experimental results of the paper to the extent that it affects the main claims and/or conclusions of the paper (regardless of whether the code and data are provided or not)?

   Answer: [Yes]

   Justification: The pipeline of the methods and the details of experiments are presented with corresponding reproducible credentials.

   Guidelines:

   - The answer NA means that the paper does not include experiments.
   - If the paper includes experiments, a No answer to this question will not be perceived well by the reviewers: Making the paper reproducible is important, regardless of whether the code and data are provided or not.
   - If the contribution is a dataset and/or model, the authors should describe the steps taken to make their results reproducible or verifiable.
   - Depending on the contribution, reproducibility can be accomplished in various ways. For example, if the contribution is a novel architecture, describing the architecture fully might suffice, or if the contribution is a specific model and empirical evaluation, it may be necessary to either make it possible for others to replicate the model with the same dataset, or provide access to the model. In general. releasing code and data is often one good way to accomplish this, but reproducibility can also be provided via detailed instructions for how to replicate the results, access to a hosted model (e.g., in the case of a large language model), releasing of a model checkpoint, or other means that are appropriate to the research performed.
   - While NeurIPS does not require releasing code, the conference does require all submissions to provide some reasonable avenue for reproducibility, which may depend on the nature of the contribution. For example
     (a) If the contribution is primarily a new algorithm, the paper should make it clear how to reproduce that algorithm.
     (b) If the contribution is primarily a new model architecture, the paper should describe the architecture clearly and fully.
     (c) If the contribution is a new model (e.g., a large language model), then there should either be a way to access this model for reproducing the results or a way to reproduce the model (e.g., with an open-source dataset or instructions for how to construct the dataset).
     (d) We recognize that reproducibility may be tricky in some cases, in which case authors are welcome to describe the particular way they provide for reproducibility. In the case of closed-source models, it may be that access to the model is limited in some way (e.g., to registered users), but it should be possible for other researchers to have some path to reproducing or verifying the results.

5. **Open access to data and code**

   Question: Does the paper provide open access to the data and code, with sufficient instructions to faithfully reproduce the main experimental results, as described in supplemental material?

   Answer: [Yes]

   Justification: All utilized data are sourced from open-access platforms. The code, which will be made publicly available, is uploaded as a zip file.

   Guidelines:

   - The answer NA means that paper does not include experiments requiring code.
   - Please see the NeurIPS code and data submission guidelines (`https://nips.cc/public/guides/CodeSubmissionPolicy`) for more details.
   - While we encourage the release of code and data, we understand that this might not be possible, so "No" is an acceptable answer. Papers cannot be rejected simply for not including code, unless this is central to the contribution (e.g., for a new open-source benchmark).

- The instructions should contain the exact command and environment needed to run to reproduce the results. See the NeurIPS code and data submission guidelines (`https://nips.cc/public/guides/CodeSubmissionPolicy`) for more details.
- The authors should provide instructions on data access and preparation, including how to access the raw data, preprocessed data, intermediate data, and generated data, etc.
- The authors should provide scripts to reproduce all experimental results for the new proposed method and baselines. If only a subset of experiments are reproducible, they should state which ones are omitted from the script and why.
- At submission time, to preserve anonymity, the authors should release anonymized versions (if applicable).
- Providing as much information as possible in supplemental material (appended to the paper) is recommended, but including URLs to data and code is permitted.

6. **Experimental setting/details**

   Question: Does the paper specify all the training and test details (e.g., data splits, hyperparameters, how they were chosen, type of optimizer, etc.) necessary to understand the results?

   Answer: [Yes]

   Justification: The pipeline of the methods and the details of experiments are presented with corresponding reproducible credentials.

   Guidelines:

   - The answer NA means that the paper does not include experiments.
   - The experimental setting should be presented in the core of the paper to a level of detail that is necessary to appreciate the results and make sense of them.
   - The full details can be provided either with the code, in appendix, or as supplemental material.

7. **Experiment statistical significance**

   Question: Does the paper report error bars suitably and correctly defined or other appropriate information about the statistical significance of the experiments?

   Answer: [Yes]

   Justification: The results contain the standard deviation of the results over several random runs.

   Guidelines:

   - The answer NA means that the paper does not include experiments.
   - The authors should answer "Yes" if the results are accompanied by error bars, confidence intervals, or statistical significance tests, at least for the experiments that support the main claims of the paper.
   - The factors of variability that the error bars are capturing should be clearly stated (for example, train/test split, initialization, random drawing of some parameter, or overall run with given experimental conditions).
   - The method for calculating the error bars should be explained (closed form formula, call to a library function, bootstrap, etc.)
   - The assumptions made should be given (e.g., Normally distributed errors).
   - It should be clear whether the error bar is the standard deviation or the standard error of the mean.
   - It is OK to report 1-sigma error bars, but one should state it. The authors should preferably report a 2-sigma error bar than state that they have a 96% CI, if the hypothesis of Normality of errors is not verified.
   - For asymmetric distributions, the authors should be careful not to show in tables or figures symmetric error bars that would yield results that are out of range (e.g. negative error rates).
   - If error bars are reported in tables or plots, The authors should explain in the text how they were calculated and reference the corresponding figures or tables in the text.

8. **Experiments compute resources**

   Question: For each experiment, does the paper provide sufficient information on the computer resources (type of compute workers, memory, time of execution) needed to reproduce the experiments?

   Answer: [Yes]

   Justification: The details of experiments are presented with corresponding reproducible credentials.

   Guidelines:

   - The answer NA means that the paper does not include experiments.

- The paper should indicate the type of compute workers CPU or GPU, internal cluster, or cloud provider, including relevant memory and storage.
- The paper should provide the amount of compute required for each of the individual experimental runs as well as estimate the total compute.
- The paper should disclose whether the full research project required more compute than the experiments reported in the paper (e.g., preliminary or failed experiments that didn't make it into the paper).

9. **Code of ethics**

   Question: Does the research conducted in the paper conform, in every respect, with the NeurIPS Code of Ethics `https://neurips.cc/public/EthicsGuidelines`?

   Answer: [Yes]

   Justification: The research conducted in the paper conforms with the NeurIPS Code of Ethics

   Guidelines:

   - The answer NA means that the authors have not reviewed the NeurIPS Code of Ethics.
   - If the authors answer No, they should explain the special circumstances that require a deviation from the Code of Ethics.
   - The authors should make sure to preserve anonymity (e.g., if there is a special consideration due to laws or regulations in their jurisdiction).

10. **Broader impacts**

    Question: Does the paper discuss both potential positive societal impacts and negative societal impacts of the work performed?

    Answer: [NA]

    Justification: There is no societal impact of the work performed.

    Guidelines:

    - The answer NA means that there is no societal impact of the work performed.
    - If the authors answer NA or No, they should explain why their work has no societal impact or why the paper does not address societal impact.
    - Examples of negative societal impacts include potential malicious or unintended uses (e.g., disinformation, generating fake profiles, surveillance), fairness considerations (e.g., deployment of technologies that could make decisions that unfairly impact specific groups), privacy considerations, and security considerations.
    - The conference expects that many papers will be foundational research and not tied to particular applications, let alone deployments. However, if there is a direct path to any negative applications, the authors should point it out. For example, it is legitimate to point out that an improvement in the quality of generative models could be used to generate deepfakes for disinformation. On the other hand, it is not needed to point out that a generic algorithm for optimizing neural networks could enable people to train models that generate Deepfakes faster.
    - The authors should consider possible harms that could arise when the technology is being used as intended and functioning correctly, harms that could arise when the technology is being used as intended but gives incorrect results, and harms following from (intentional or unintentional) misuse of the technology.
    - If there are negative societal impacts, the authors could also discuss possible mitigation strategies (e.g., gated release of models, providing defenses in addition to attacks, mechanisms for monitoring misuse, mechanisms to monitor how a system learns from feedback over time, improving the efficiency and accessibility of ML).

11. **Safeguards**

    Question: Does the paper describe safeguards that have been put in place for responsible release of data or models that have a high risk for misuse (e.g., pretrained language models, image generators, or scraped datasets)?

    Answer: [Yes]

    Justification: Released models that have a high risk for misuse or dual-use should be released with necessary safeguards to allow for controlled use of the model, by requiring that users adhere to usage guidelines or restrictions to access the model or implementing safety filters.

    Guidelines:

    - The answer NA means that the paper poses no such risks.

- Released models that have a high risk for misuse or dual-use should be released with necessary safeguards to allow for controlled use of the model, for example by requiring that users adhere to usage guidelines or restrictions to access the model or implementing safety filters.
- Datasets that have been scraped from the Internet could pose safety risks. The authors should describe how they avoided releasing unsafe images.
- We recognize that providing effective safeguards is challenging, and many papers do not require this, but we encourage authors to take this into account and make a best faith effort.

12. **Licenses for existing assets**

    Question: Are the creators or original owners of assets (e.g., code, data, models), used in the paper, properly credited and are the license and terms of use explicitly mentioned and properly respected?

    Answer: [Yes]

    Justification: The original owners of assets, including data and models, used in the paper, are properly credited and are the license and terms of use explicitly mentioned and properly respected.

    Guidelines:

    - The answer NA means that the paper does not use existing assets.
    - The authors should cite the original paper that produced the code package or dataset.
    - The authors should state which version of the asset is used and, if possible, include a URL.
    - The name of the license (e.g., CC-BY 4.0) should be included for each asset.
    - For scraped data from a particular source (e.g., website), the copyright and terms of service of that source should be provided.
    - If assets are released, the license, copyright information, and terms of use in the package should be provided. For popular datasets, `paperswithcode.com/datasets` has curated licenses for some datasets. Their licensing guide can help determine the license of a dataset.
    - For existing datasets that are re-packaged, both the original license and the license of the derived asset (if it has changed) should be provided.
    - If this information is not available online, the authors are encouraged to reach out to the asset's creators.

13. **New assets**

    Question: Are new assets introduced in the paper well documented and is the documentation provided alongside the assets?

    Answer: [Yes]

    Justification: The new assets introduced in the paper are well documented and provided alongside the assets.

    Guidelines:

    - The answer NA means that the paper does not release new assets.
    - Researchers should communicate the details of the dataset/code/model as part of their submissions via structured templates. This includes details about training, license, limitations, etc.
    - The paper should discuss whether and how consent was obtained from people whose asset is used.
    - At submission time, remember to anonymize your assets (if applicable). You can either create an anonymized URL or include an anonymized zip file.

14. **Crowdsourcing and research with human subjects**

    Question: For crowdsourcing experiments and research with human subjects, does the paper include the full text of instructions given to participants and screenshots, if applicable, as well as details about compensation (if any)?

    Answer: [NA]

    Justification: The answer NA means that the paper does not involve crowdsourcing nor research with human subjects.

    Guidelines:

    - The answer NA means that the paper does not involve crowdsourcing nor research with human subjects.
    - Including this information in the supplemental material is fine, but if the main contribution of the paper involves human subjects, then as much detail as possible should be included in the main paper.

- According to the NeurIPS Code of Ethics, workers involved in data collection, curation, or other labor should be paid at least the minimum wage in the country of the data collector.

15. **Institutional review board (IRB) approvals or equivalent for research with human subjects**

    Question: Does the paper describe potential risks incurred by study participants, whether such risks were disclosed to the subjects, and whether Institutional Review Board (IRB) approvals (or an equivalent approval/review based on the requirements of your country or institution) were obtained?

    Answer: [NA]

    Justification: The answer NA means that the paper does not involve crowdsourcing nor research with human subjects.

    Guidelines:

    - The answer NA means that the paper does not involve crowdsourcing nor research with human subjects.
    - Depending on the country in which research is conducted, IRB approval (or equivalent) may be required for any human subjects research. If you obtained IRB approval, you should clearly state this in the paper.
    - We recognize that the procedures for this may vary significantly between institutions and locations, and we expect authors to adhere to the NeurIPS Code of Ethics and the guidelines for their institution.
    - For initial submissions, do not include any information that would break anonymity (if applicable), such as the institution conducting the review.

16. **Declaration of LLM usage**

    Question: Does the paper describe the usage of LLMs if it is an important, original, or non-standard component of the core methods in this research? Note that if the LLM is used only for writing, editing, or formatting purposes and does not impact the core methodology, scientific rigorousness, or originality of the research, declaration is not required.

    Answer: [Yes]

    Justification: The core method development in this research dose not involve LLMs as any important, original, or non-standard components.

    Guidelines:

    - The answer NA means that the core method development in this research does not involve LLMs as any important, original, or non-standard components.
    - Please refer to our LLM policy (`https://neurips.cc/Conferences/2025/LLM`) for what should or should not be described.